

Č. Branković · D. Gregory

Impact of horizontal resolution on seasonal integrations

Received: 11 August 2000 / Accepted: 13 February 2001

Abstract The effects of changing horizontal resolution are studied using ensembles of seasonal simulations made by a relatively recent version of the ECMWF model. The model is integrated at T63, T_L159 and T_L319 spectral resolutions. The last corresponds approximately to a 0.56° latitude-longitude grid and may be considered, by climate modelling standards, as very high resolution. Though, on average, no dramatically large differences in ensemble mean quantities are found between the three resolutions, some monotonic (systematic) differences with increasing resolution are evident. Whilst the better representation of orography with increasing resolution accounts for many differences between the resolutions considered, not all variations can be associated with changes in local orographic features. The existence of systematic changes with resolution indicates that the development of numerical models, especially physical parametrizations, should be carried out simultaneously at various resolutions. The study indicates that the highest model resolution does not always give the best results in terms of verification. In addition, reanalysis parameters that are mainly driven by model physics may not be optimal for the verification in such resolution studies.

1 Introduction

The dependence of atmospheric general circulation models (AGCM) used in climate studies on horizontal resolution is a subject of continuous interest. Despite a

constant increase in computational power, various compromises in model formulation and/or horizontal resolution are normally made for reasons of computational efficiency. The issue of horizontal resolution has become even more important as many centres have adopted a probabilistic approach to seasonal forecasting, i.e. in an operational environment ensembles of forecasts are made on a (quasi) regular basis. Coupled to ocean models, these multiple long-range AGCM integrations pose a substantial demand on computational resources. Therefore computationally efficient and yet physically and numerically adequate model horizontal resolution is a matter of a great importance.

There are a number of studies dealing explicitly with the topic of AGCM horizontal resolution in extended or long-range integrations. The increase in computational power has made the horizontal resolutions considered in some earlier studies to be very low by present standards (e.g. Boer and Lazare 1988). At the European Centre for Medium-Range Weather Forecasts (ECMWF), the impact of horizontal resolution on systematic errors at monthly time scales was extensively studied by Tibaldi et al. (1990), comparing four different spectral resolutions: T21, T42, T63 and T106. Errors in mean fields were reduced as horizontal resolution increased. The largest differences were often found in the detailed structure of various parameters. They concluded that parameters or processes related to the representation of orography, such as precipitation, might benefit from higher model resolutions.

Williamson et al. (1995) found for many climate statistics a monotonic signal with increasing resolution in the NCAR model. The largest variation in these statistics was occurring at low resolutions (R15 and T21) and smallest variation occurring at medium resolutions (T42 and T63). They also found that the highest resolution does not always produce the results closest to verifying analysis. Based on integrations from an earlier version of the ECMWF model, Boyle (1993) came to similar conclusions. Phillips et al. (1995) ascertained that for moist processes, the pattern established at the T42

Č. Branković (✉)¹ · D. Gregory²
ECMWF, Shinfield Park, Reading,
RG2 9AX, United Kingdom
E-mail: cedob@ictp.trieste.it

Current affiliations:

¹The Abdus Salam International Centre for Theoretical Physics
Strada Costiera 11, 34014 Trieste, Italy

²Met Office, Hadley Centre for Climate Prediction and Change,
London Road, Bracknell, RG12 2SY, United Kingdom

resolution carries over to higher resolutions with incremental variations.

Déqué and Pielieuvre (1995) claim that the stretched grid, of T200 over the domain of interest (Europe) and T21 over the southern Pacific, is a valid alternative to model nesting. Stratton (1999) compared the results from relatively high horizontal resolution (0.833° latitude by 1.25° longitude) with coarser resolution in 10-year integrations of the Hadley Centre climate model (HadAM2b). She found that the increase in horizontal resolution improved the model's cold bias in the troposphere and generally increases the variability of the model. Whereas there is a general consensus that higher horizontal resolution generally has a beneficial impact on systematic model behaviour, some studies revealed problems, previously unnoticed, when the horizontal resolution was increased (e.g. Palmer et al. 1986).

Here the effects of increasing horizontal resolution are studied using ensembles of seasonal simulations made by a relatively recent version of the ECMWF model. The main objective is twofold. First, we consider whether the convergence of model results (errors) on seasonal time scales could be attained when horizontal resolutions used are much higher than those considered in previous studies. It will be shown that this is not always the case. Second, we consider whether the differences in horizontal resolutions (and ultimately in systematic errors) have relevance to the methodology commonly used to develop both physics and dynamics components of forecast (climate) models. A typical example is testing low-resolution configurations of a model for development prior to implementation at higher resolution. This approach may not be optimal to reduce errors or climate drift at higher resolution.

In the next section, a brief description of experimental strategy is given. In Sect. 3, mean errors in upper-air fields are discussed focusing on extratropical circulation. For many parameters, a *t*-test is performed to ascertain whether the ensemble mean for a given resolution is, in a statistical sense, significantly different from the ensemble mean of any other resolution; these results are discussed in Sect. 4. In Sect. 5, some results related to the tropical large-scale circulation are presented. The impact of model resolution on precipitation and some other surface parameters is discussed in Sect. 6 and some concluding remarks are made in Sect. 7.

2 Experimental design

2.1 Model and experiments

For the purpose of this study, the ECMWF model was integrated at T63, T_L159 and T_L319 spectral resolutions. In comparison with most previous studies in the extended-range, these resolutions, in particular T_L319, provide a substantial increase in model horizontal resolution. In the grid-point space, the T_L319 spectral resolution effectively corresponds to approximately 0.56° by 0.56° latitude/longitude grid, even higher than the one used by Stratton (1999). The numerical scheme was semi-Lagrangian, and for all

resolutions, the computation in grid-point space was performed on the reduced Gaussian grid (see, e.g. Hortal and Simmons 1991). The reduced grid is more isotropic in comparison to the full Gaussian grid, and performs fewer computations at middle and polar latitudes. The subscript L in T_L159 and T_L319 relates to the linear grid on which the physics parameters are computed (Hortal 1999).

The model version used for the integrations discussed was 18R6 with 31 levels in the vertical. A detailed description of major model modifications prior to this cycle is given in Gregory et al. (2000). This model cycle was used in ECMWF medium-range operations from June 1998 to March 1999 at the T_L319 resolution.

The six-member ensembles were run for one summer (1987) and for one winter season (1987/88). Summer runs were initiated on and around 1 May, winter ones on and around 1 November. The initial data and sea surface temperatures (SSTs) were taken from ECMWF archive. The SSTs were updated daily in the model. Although only one season is used from a particular year, experience suggests this is sufficient to gain understanding of mean model biases. However, this is insufficient to make definite statements concerning the effect of resolution on the representation of the annual cycle or interannual variability.

The ensemble size (six members) used in this study was dictated primarily by computational requirements for the T_L319 resolution. However, where appropriate, for both T63 and T_L159, a brief discussion on the impact of increased ensemble size to nine members is given. In addition, we also analyzed the impact of coupling of the ECMWF wave and atmospheric models, given that the wave model is an intrinsic part of ECMWF forecasting system (see, e.g. Janssen and Viterbo 1996 for the description of the ECMWF wave model). For technical reasons, use of the wave model was not possible at T_L319, but the impact of the wave model at T63 and T_L159 resolutions is discussed.

For each resolution, seasonal ensemble averages were computed for conventional Northern Hemisphere summer, June to August (JJA), and winter, December to February (DJF), and compared with ECMWF reanalysis (ERA-15, Gibson et al. 1997). The spectral resolution of ERA-15 was T106. During the summer of 1987, a moderately strong El Niño event in the equatorial Pacific was observed, which subsequently weakened and almost disappeared in the following winter.

2.2 Mean ensemble spread

As mentioned, the size of ensembles was constrained primarily by computational demands for T_L319 experiments. Nevertheless, by comparing estimates of mean ensemble spread, an attempt was made to assess how a variable horizontal resolution relates to ensemble size. Such estimates of ensemble spread are based on average root-mean-square (RMS) difference over all pairs of realization within an ensemble. For a six-member ensemble, 15 differences/pairs can be computed. In Table 1, these estimates are given for 500 mb heights over three areas: extratropical Northern Hemisphere, Europe and North America. In DJF, there is a clear increase in spread from T63 to T_L159, and to T_L319, indicating possible need for larger ensembles when higher resolution is used.

Table 1 The 500 mb height mean RMS difference (in dam) for all pairs within six-member sub-ensembles for T63 and T_L159, and ensembles for T_L319 averaged for three regions. Figures in brackets for T63 and T_L159 refer to average values over all possible six-member sub-ensembles from the full nine-member ensemble

| Area | | NH | Europe | N. America |
|------|--------------------|-----------|-----------|------------|
| DJF | T63 | 3.9 (4.3) | 4.6 (5.8) | 4.1 (4.3) |
| | T _L 159 | 4.7 (4.5) | 5.5 (5.5) | 5.0 (4.5) |
| | T _L 319 | 5.0 (–) | 5.8 (–) | 5.2 (–) |
| JJA | T63 | 2.4 (2.5) | 2.9 (3.3) | 2.4 (2.4) |
| | T _L 159 | 2.5 (2.5) | 3.3 (3.1) | 2.5 (2.5) |
| | T _L 319 | 2.4 (–) | 3.3 (–) | 2.1 (–) |

Figures in brackets in Table 1 are also for six-member ensembles, but when all combinations of six-members “sub-ensembles” are considered within the nine-member ensemble (these were available for T63 and T_L159 only). In this case, the mean RMS difference for T63 is increased a little, however, except for Europe, it is still below the estimate for the T_L159 resolution. For JJA, the variation in the mean RMS difference among the resolutions is very small and no clear signal can be implied from Table 1. This essentially confirms that the size of seasonal ensembles will also depend on season, parameter, and area considered as discussed by Branković and Palmer (1997).

3 Upper air fields

Many results in this and following sections are analyzed and presented in terms of ensemble mean errors with respect to ERA-15 data. Although analysis of model errors is not the main objective of this study, this approach enables assessment of relative performance of one resolution with respect to the others.

3.1 Height and wind errors

Figure 1 shows the DJF 1987/88 500 mb height ensemble mean errors with respect to ERA-15 for the three resolutions together with the reference reanalysis full field. The mainly negative mean height errors which dominate over the Northern Hemisphere at T63 are generally reduced at both T_L159 and T_L319 (Fig. 1, left panels). This reduction is most pronounced over the Rockies and Himalayas and may be related to better representation of orography as the horizontal resolution increases.

Whereas the westerly bias over the north Pacific (associated with a poleward geopotential height gradient over the region) is monotonically reduced with resolution, over the north Atlantic and western Europe it is increased somewhat at T_L159 relative to T63, but at T_L319 reduces to become smaller than at T63. On the other hand, the amplitude of positive errors over Japan and eastern Asia increases monotonically from T63 to T_L319, though the area of error is largest at T_L159. Compared with T63, errors in the tropics and southern mid-latitudes have been also reduced in both T_L159 and T_L319 models, but increased over Antarctica (Fig. 1, right panels). Bearing in mind the reduction of errors with increased resolution over the Himalayas and the Rockies, the increase in error amplitude over Antarctica at higher resolutions seems puzzling. Boyle (1993) found an error increase with increased resolution in the Southern Hemisphere stationary waves. However, he could not explain the cause of these errors and speculated that erroneous stationary waves could have been forced by a strong tropical convection.

Such a mixed change in error pattern with resolution is not fully understood, and one might be tempted to ascribe it to a limited sampling. Figure 2a–d shows the DJF 1987/88 500 mb height mean errors for T63 and T_L159 respectively when ensemble size was increased from six to nine members. For both resolutions,

although the (Northern Hemisphere) mean errors are in general slightly reduced when ensemble size increases, the mean response remains essentially unchanged (see Fig. 1a–d).

In JJA 1987, the dominant negative error over Antarctica at T63, and to a lesser extent at T_L159, has been replaced by relatively large positive error at T_L319 (not shown). It is not clear whether this change in the sign of the T_L319 error over Antarctica could be solely ascribed to a higher orography with T_L319 in comparison with the other two resolutions. The differences between T_L319 and T_L159 orographies are mainly of the small spatial scale and are confined to the Antarctica coastal regions with the maximum difference of around 500 m on the Antarctica peninsula (60°W). In the tropics, T_L159 exhibits largest positive errors among the three resolutions.

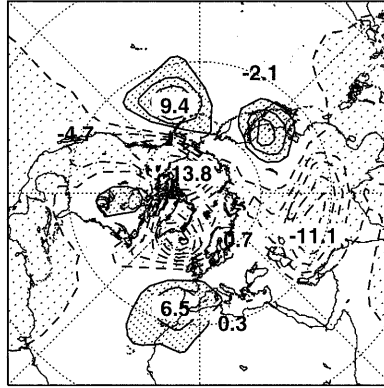
Errors in zonally averaged zonal wind (*u*-wind) are shown in Fig. 3. In the northern winter, errors are reduced as the model resolution increases (left panels), while in the southern winter, errors worsen with the resolution (right panels). An increase in the near tropopause errors with resolution can also be seen in the tropics during JJA. At T_L319, this deterioration of the tropical *u*-wind error is associated with an increase in easterlies near the tropopause. A large positive JJA error between 25°S and 45°S, found in all resolutions, is related to an erroneous overestimation of the subtropical jet by nearly 15%. It is interesting to note that, despite this increase in zonally averaged *u*-wind error with resolution in the southern subtropics, the longitudinally varying *u*-wind error at 200 mb is largest at T63 (21 ms⁻¹), and smallest at T_L319 (16 ms⁻¹; not shown).

The increase in *u*-wind error with resolution in the Southern Hemisphere winter (JJA; Fig. 3) is difficult to explain. These errors resemble, to a certain extent, to those described by Boyle (1993), though in our case they are shifted equatorward and are of smaller amplitude. They might be thought of being associated with, e.g., less efficient parametrization of the gravity wave drag (GWD) in the Southern Hemisphere as resolution increases. In the ECMWF model, the coefficients related to the GWD parametrization are not changed with increasing resolution, and the efficiency of the GWD parametrization is associated with (increased) effects of the sub-grid scale orography. In the latitudinal belt where the *u*-wind error is largest (20°S to 45°S), only the Andes contain important orographic (and consequently sub-grid scale) features, which however, may be insufficient to damp increasing winds with increased resolution. The other possible candidate to cause such an error might be inadequate vertical resolution near the tropopause. In any case, more experimentation would be required to clarify and explain such model errors.

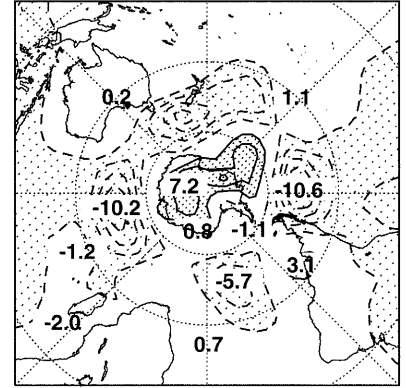
The underestimation of (zonally averaged) eddy kinetic energy found in earlier versions of ECMWF low resolution models (as reported in, e.g. Tibaldi et al. 1990) is also found at T63 in both hemispheres and both seasons (Fig. 4, top panels). In the Northern Hemi-

Fig. 1 a, b DJF 1987/88 ensemble mean 500 mb geopotential height error fields for T63, **c, d** for T_L159, **e, f** for T_L319, **g, h** ERA-15 full field. Contours: 2 dam for error fields and 10 dam for the full field. Positive errors: *dense stipple*; negative errors: *coarse stipple*

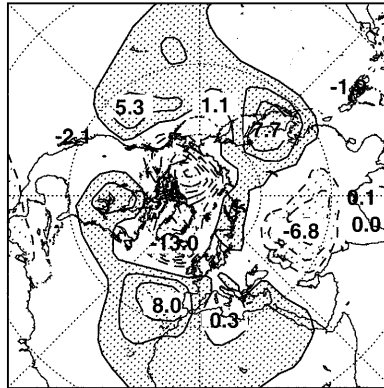
a) Z500 error T63 (6), DJF 1987/88; cont = 2 dam



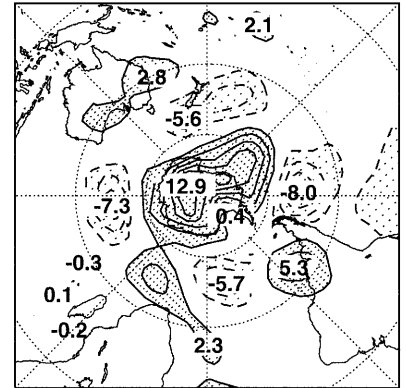
b) Z500 error T63 (6), DJF 1987/88; cont = 2 dam



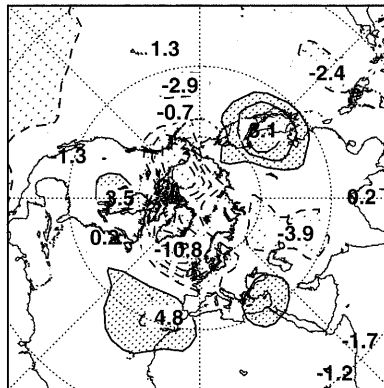
c) Z500 error T159 (6), DJF 1987/88; cont = 2 dam



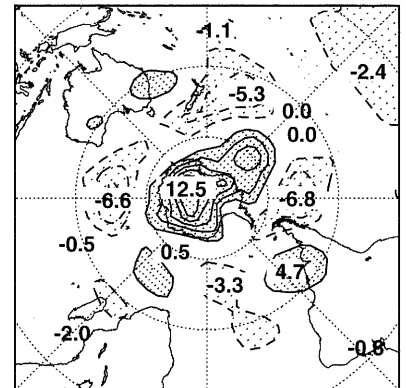
d) Z500 error T159 (6), DJF 1987/88; cont = 2 dam



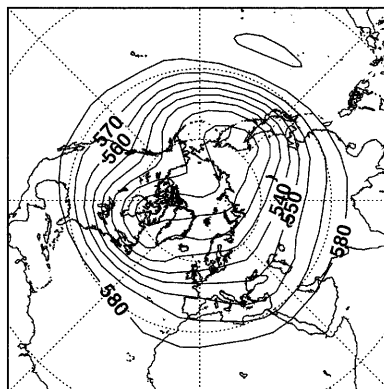
e) Z500 error T319 (6), DJF 1987/88; cont = 2 dam



f) Z500 error T319 (6), DJF 1987/88; cont = 2 dam



g) Z500 ERA, DJF 1987/88; cont = 10 dam



h) Z500 ERA, DJF 1987/88; cont = 10 dam

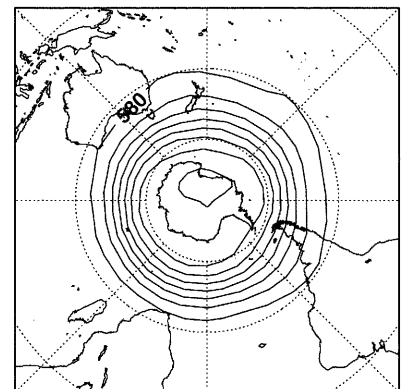
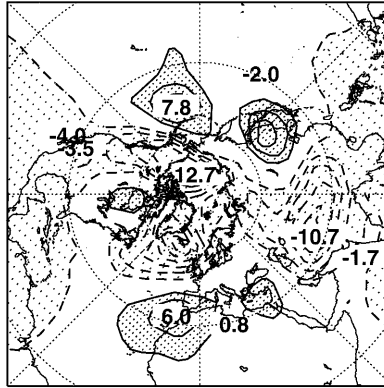
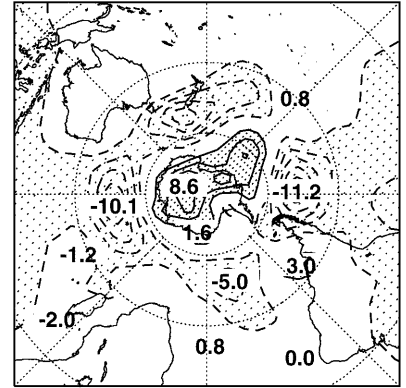


Fig. 2 As Fig. 1, but when ensemble size was increased to nine members **a, b** for T63, **c, d** for T_L159, **e, f** when wave model was coupled to the atmospheric model for T63, **g, h** for T_L159. Contours: 2 dam; positive errors: *dense stipple*, negative errors: *coarse stipple*

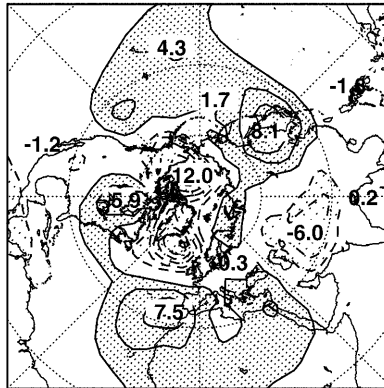
a) Z500 error T63 (9), DJF 1987/88; cont = 2 dam



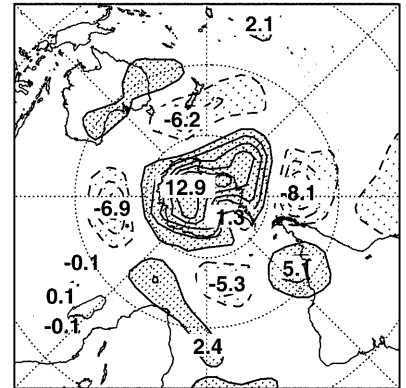
b) Z500 error T63 (9), DJF 1987/88; cont = 2 dam



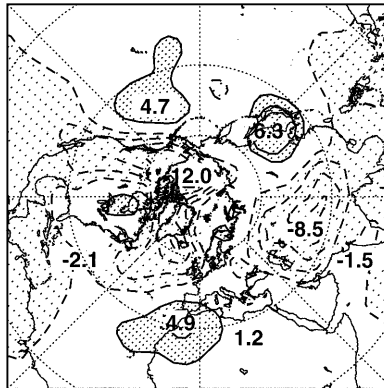
c) Z500 error T159 (9), DJF 1987/88; cont = 2 dam



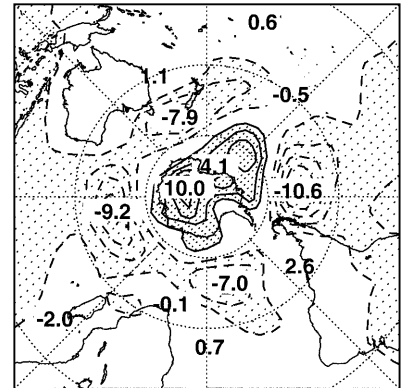
d) Z500 error T159 (9), DJF 1987/88; cont = 2 dam



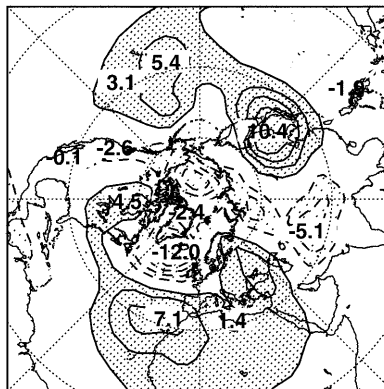
e) Z500 error T63 (6) wave, DJF 1987/88; cont = 2 dam



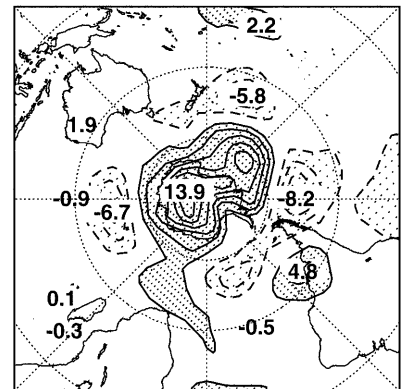
f) Z500 error T63 (6) wave, DJF 1987/88; cont = 2 dam



g) Z500 error T159 (6) wave, DJF 1987/88; cont = 2 dam



h) Z500 error T159 (6) wave, DJF 1987/88; cont = 2 dam



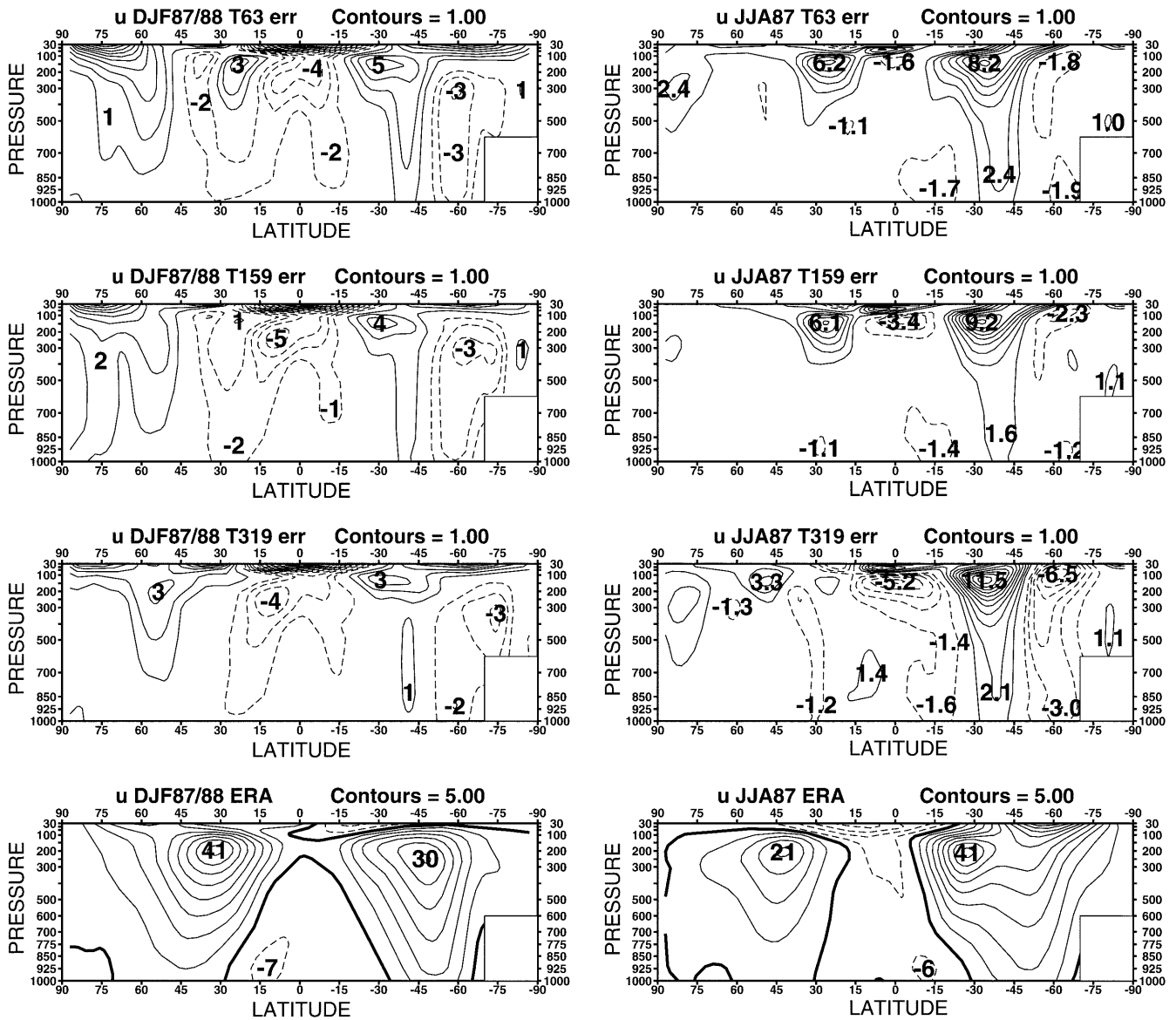


Fig. 3 Zonally averaged u -wind ensemble mean errors for DJF 1987/88 (left) and JJA 1987 (right). From top to bottom: T63, T_{L159} , T_{L319} errors respectively and ERA-15 full field. Contours: 1 ms^{-1} for errors and 5 ms^{-1} for full fields. Negative errors and easterlies dashed

sphere, this deficiency is gradually reduced as the model resolution increases. In the Southern Hemisphere, eddy kinetic energy is too large at T_{L319} relative to ERA-15, the maximum error being confined to midlatitudes. The energy increase in T_{L319} is larger in the southern summer (DJF) than in winter.

The reasons for somewhat different model responses over the Northern and Southern Hemispheres shown in Fig. 4 are not quite obvious. In order to shed some light on such different error patterns, zonally averaged eddy momentum fluxes (meridional and vertical), as well as eddy heat flux were analyzed (not shown). For both eddy meridional momentum flux, u^*v^* , and eddy heat flux, v^*T^* , no major difference among various resolutions is seen. For eddy vertical momentum flux, w^*u^* , an increase at T_{L319} of about 50% relative to the other resolutions and to ERA-15 was found in JJA at the edge

of Antarctica, around 65°S . This may have contributed to an erroneous increase in eddy kinetic energy (Fig. 4 right panels), since the conversion from zonal kinetic energy to eddy kinetic energy is proportional to w^*u^* (Lorenz 1967). This increase in w^*u^* coincides with an increase in w variance and could be ultimately linked to the effect of increased Antarctica's coastal orography at the highest resolution (see also earlier comments on the differences in Antarctica's orography).

3.2 Frequency of blocking

In Fig. 5a, the wintertime (DJF) Northern Hemisphere frequency of blocking occurrence for the three resolutions is shown. For the definition of blocking and frequency of occurrence, the same criteria as in Tibaldi

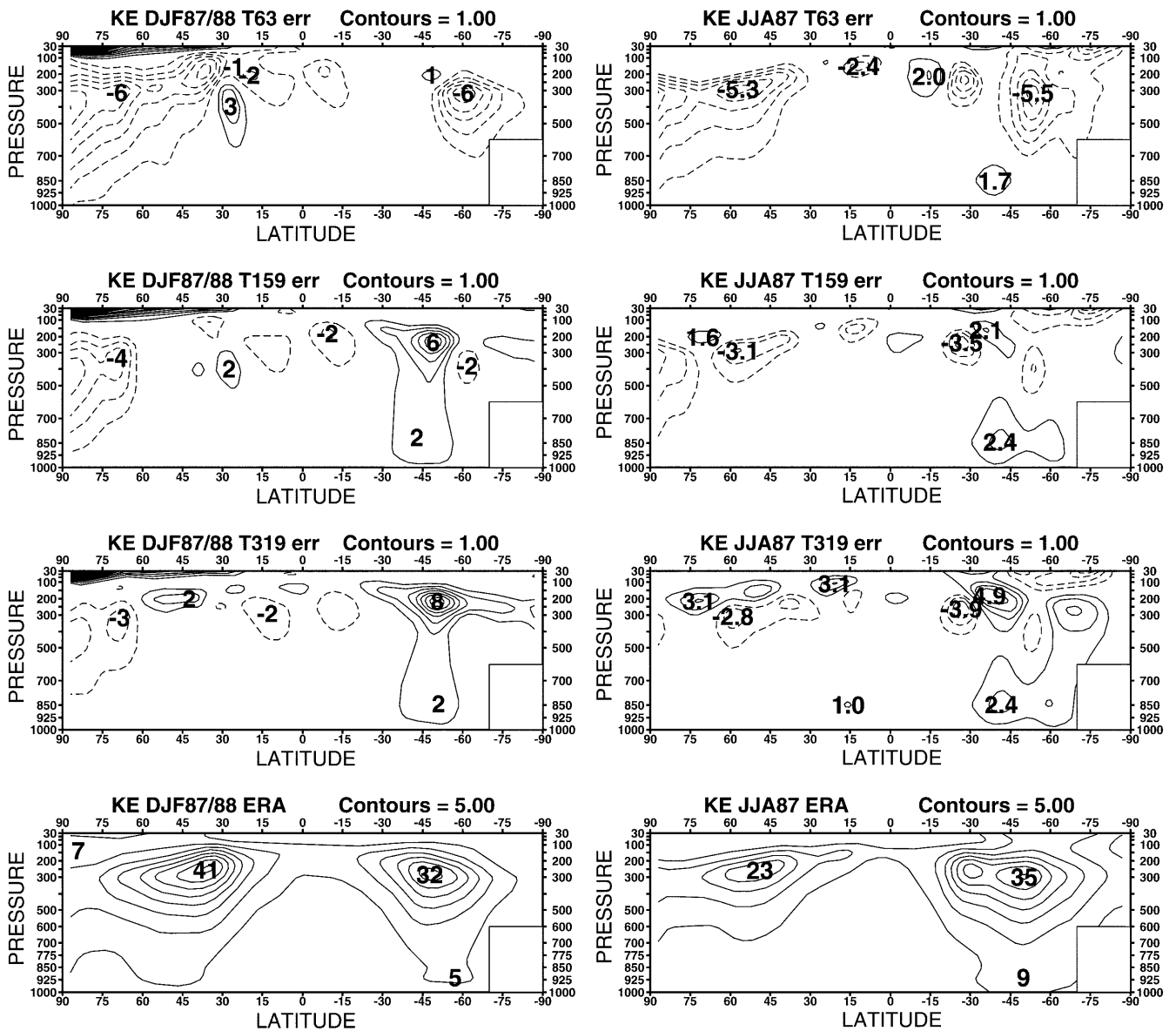


Fig. 4 As Fig. 3 but for eddy kinetic energy. Units are J/(m²Pa). Negative errors dashed

and Molteni (1990) were used. The model results are compared against the mean frequency derived from the seven ERA-15 winters with non-significant El Niño-Southern Oscillation (ENSO) index (heavy solid line). The mean observed blocking frequency is used for comparison here, because only one non-ENSO winter (DJF 1987/88) is not representative of climatological blocking frequency. These non-ENSO winters include the following: 1979/80, 1980/81, 1981/82, 1987/88, 1989/90, 1990/91 and 1992/93 (see, e.g., Branković and Palmer 2000 for the classification of ERA-15 seasons into ENSO and non-ENSO).

In all models, the peak frequencies for Atlantic/European block are found further east of its climatological maximum (see also Tibaldi and Molteni 1990). A very likely cause for such a downstream displacement is the non-negligible westerly bias over the north Atlantic

already discussed. No major differences among the models are seen, though the higher resolutions tend to produce blocks over a larger geographical (longitudinal) area than T63. The modelled blocking frequency at all resolutions is underestimated when compared with the observed “climate”.

Over the Pacific, the modelled blocking frequency is again underestimated when compared with observations. At T63 and T_L319, the frequency is about twice as large as at T_L159. When the ensemble size is increased to nine members, the frequency of blocks at T_L159 increases a little, but is still below the other resolutions (not shown). Thus the sampling may have some influence on the blocking frequency, but it is still not clear what may have caused such behaviour at T_L159. For T63 simulations, no major effect on blocking frequency due to increased ensemble size is found.

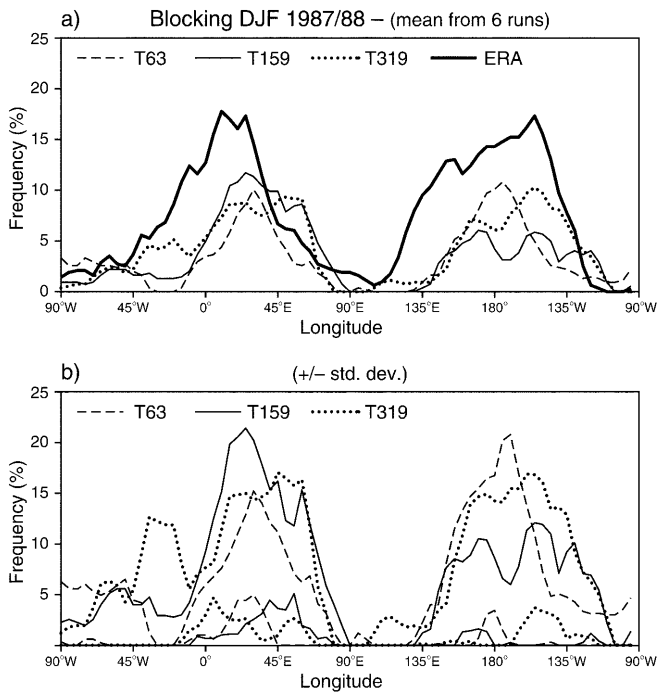


Fig. 5a, b Frequency of blocking occurrence in % in DJF 1987/88 for **a** six-member ensembles for T63 (thin dashed), T_L159 (thin solid), T_L319 (thin dotted) resolutions, and for seven non-ENSO ERA-15 winters (heavy solid); **b** ± 1 standard deviation of the mean blocking frequency from six-member ensembles

In Fig. 5b, the two curves for each resolution indicate the ± 1 standard deviation of the mean blocking frequency from six-member ensembles. Over the Atlantic sector, there is no significant difference (in the statistical sense) between the three resolutions considered, i.e. the areas enveloped by different resolutions overlap to a great extent. For the Pacific sector we consider the two following longitudes: first, at around 150°W, where the observed climate and both higher resolutions display maximum blocking frequency (albeit with different amplitudes), and second, at around 180° where T63 displays maximum frequency. At 150°W, there is no significant difference between T_L159 and other resolutions, but T63 and T_L319 are statistically different. At the date line, T_L159 is “just” statistically different from T63, but statistically equal to T_L319. Therefore, we may assume that, in terms of blocking frequency statistics, the T_L159 resolution is not significantly different from the other two resolutions.

The difference in the positioning of the T63 and T_L319 Pacific blocking might be attributed to a better representation of the Rocky Mountains in the highest resolution model. The ridge over the Rockies is stronger at T_L319 than at T63 (not shown, but see Fig. 1 where the 500 mb height error over the Rockies is greatly reduced at T_L319). This stronger ridging at T_L319 causes the upstream flow over the eastern extratropical Pacific to be more diffluent than at T63. Consequently, such a stronger diffluence may effect more favourable conditions for blocking development than relatively strong zonal flow

seen at T63. The same argument could be applied to T_L159, since Fig. 1c also shows a reduction in the height error over the Rockies when compared with T63. Indeed, there is a (secondary) peak in T_L159 at around 150°W, and as Fig. 5b and the discussion above show, this peak is not significantly different from that at T_L319.

3.3 Temperature errors

An erroneous northern wintertime cooling of the high-latitude troposphere is gradually reduced from T63 to T_L319, but remains almost unchanged in the polar stratosphere (Fig. 6 left). In northern summer, the largest erroneous warming is found at T_L319 in the lower troposphere (Fig. 6 right). Thus, in both seasons, there seems to be a monotonic increase in the Northern Hemisphere lower tropospheric temperature as the model resolution increases. Whereas this has a beneficial effect on mean error in northern winter, it causes the deterioration of temperature error in northern summer. Similar behaviour is also seen in the Southern Hemisphere, however, with smaller amplitude.

The warming of the troposphere with increasing resolution has been also noted in some other studies, for example, Stratton (1999), Williamson et al. (1995). Stratton (1999) attributes the effect to the increased intensity of the hydrological cycle at higher resolution due to more intense vertical motion (see comments on precipitation changes later).

It is not clear whether an erroneous warming at low levels in JJA could be linked to land surface processes. For example, at 850 mb, temperature errors are almost equally spread over both land and sea (sea-ice) points of the Northern Hemisphere high latitudes (not shown). Changes to cloud amounts might be thought to play a role, but low-level cloud amounts are similar at all resolutions over the high latitudes of the Northern Hemisphere. For mid-level clouds, a decrease in cloud amount in this region is found as resolution increases. Errors in the poleward eddy heat flux in both winter hemispheres are lowest with T_L319 in mid-latitudes, the region where this flux is strongest (not shown).

The left panels in Fig. 6 (DJF) also indicate a strong stratospheric cooling in both southern and northern high latitudes. The spatial extent of this erroneous cooling is clearly seen at 200 mb (Fig. 7). At T_L319, the maximum error reaches -9 K over Antarctica, whereas at lower resolutions it is about -10 and -7 K respectively. In the Northern Hemisphere, the high-resolution model displays the largest negative stratospheric errors. Thus, in contrast to the lower troposphere, there is a net upper-air cooling as the model resolution increases (see Fig. 6 left). This strong stratospheric cooling was also evident in the earlier versions of ECMWF model (Branković and Molteni 1997), and indeed is found to be a common deficiency of many GCMs (Boer et al. 1991). Johnson (1997) describes this cold bias as a means for balancing entropy in the model atmosphere since spurious

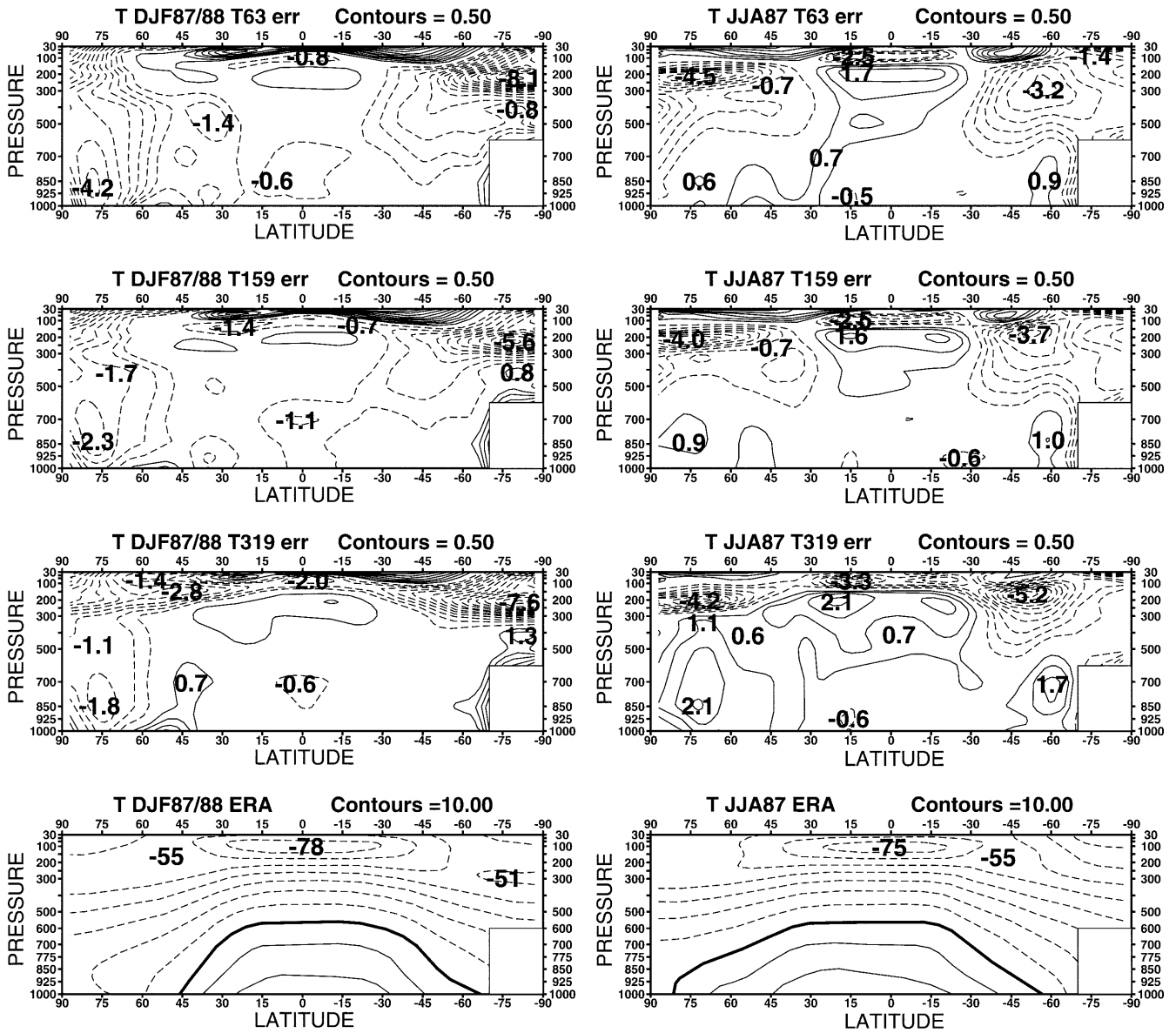


Fig. 6 As Fig. 3 but for temperature. Contours: 0.5 K for errors and 10 K for full fields. Negative errors and negative temperatures *dashed*

numerical dispersion/diffusion, Gibbs oscillation, errors in parametrization and other improperly modelled processes cause positive “aphysical” sources of entropy.

The relative similarity in the Northern Hemisphere temperature error pattern between T63 and T_L159 seen in Fig. 7, and somewhat different (larger) errors in T_L319, indicate a possible problem in the testing methodology adopted at ECMWF for the medium-range (see Gregory et al. 2000 for details). Development testing at lower resolution (T63) may not be appropriate, at least for physical parametrization, to ensure improved performance at higher resolutions.

Large positive errors in middle and low latitudes at T63 and T_L159, seen in Fig. 7, can be associated with the main large-scale orography features, the Rockies and the Tibetan plateau. However, the feature that may corre-

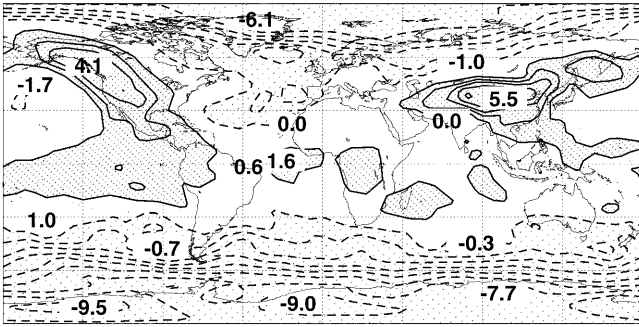
spond to the Andes is conspicuously absent here (nor is seen in JJA, the southern winter counterpart). In T_L319, these errors are reduced and confined mainly to the tropics and do not seem to be related to orography.

In JJA, in all resolutions considered, positive errors at 200 mb are dominant in the tropical regions (not shown). These positive errors are largest with T_L319. In mid and high latitudes negative errors of up to -9 K prevail in all resolutions (see also Fig. 6 right panels).

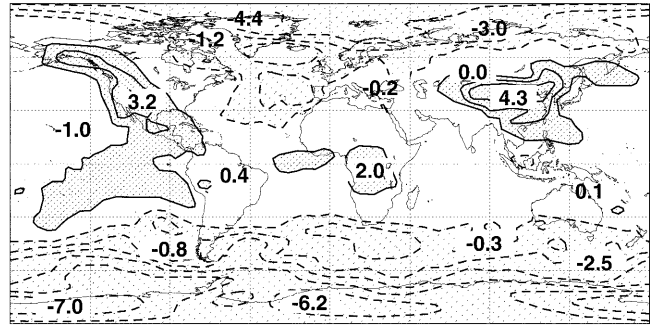
3.4 The impact of the wave model

As indicated in introduction, for lower resolution models, T63 and T_L159, ensembles of experiments were created in which the ECMWF wave model was coupled

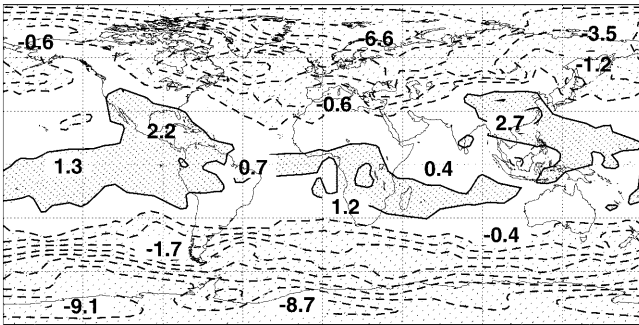
a) T200 error T63 (6), DJF 1987/88; contours = 1 deg



b) T200 error T159 (6), DJF 1987/88; contours = 1 deg



c) T200 error T319 (6), DJF 1987/88; contours = 1 deg



d) T200 ERA-15, DJF 1987/88; contours = 2 deg

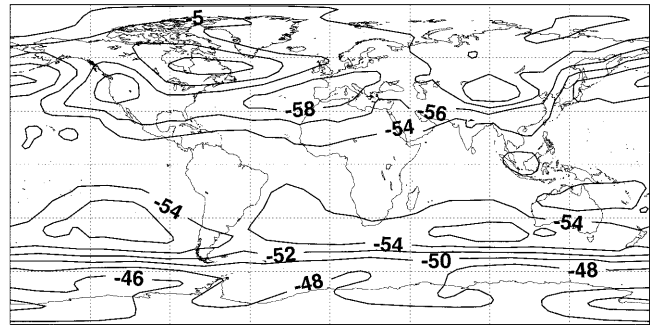


Fig. 7a–d As Fig. 1 but for the DJF 1987/88 200 mb temperature. Contours: 1 K for error fields and 2 K for the full field

to the atmospheric model. Here a brief summary of the impact of the wave model is given, focusing on six-member ensembles.

Figure 2e–h shows the DJF 1987/88 500 mb height mean errors for T63 and T_L159 when the wave model was coupled to the atmospheric model. When compared with runs without wave model (Fig. 1a–d), it can be seen that the inclusion of the wave model generally contributes to the reduction of error amplitude over much of the globe; however, the error pattern remains essentially unchanged. It seems that the impact of wave model coupling is more significant at T63 than at T_L159. For example, whereas at T63 the westerly bias over the north Atlantic is substantially reduced, at T_L159 it is reduced only marginally. Over Antarctica, the coupling of the wave model yields a somewhat deteriorating effect. Similar model response is found in JJA and for some other parameters. These results are consistent with those of Janssen and Viterbo (1996) who found a (mostly) beneficial impact of ocean waves on the climatology of an earlier version of ECMWF model.

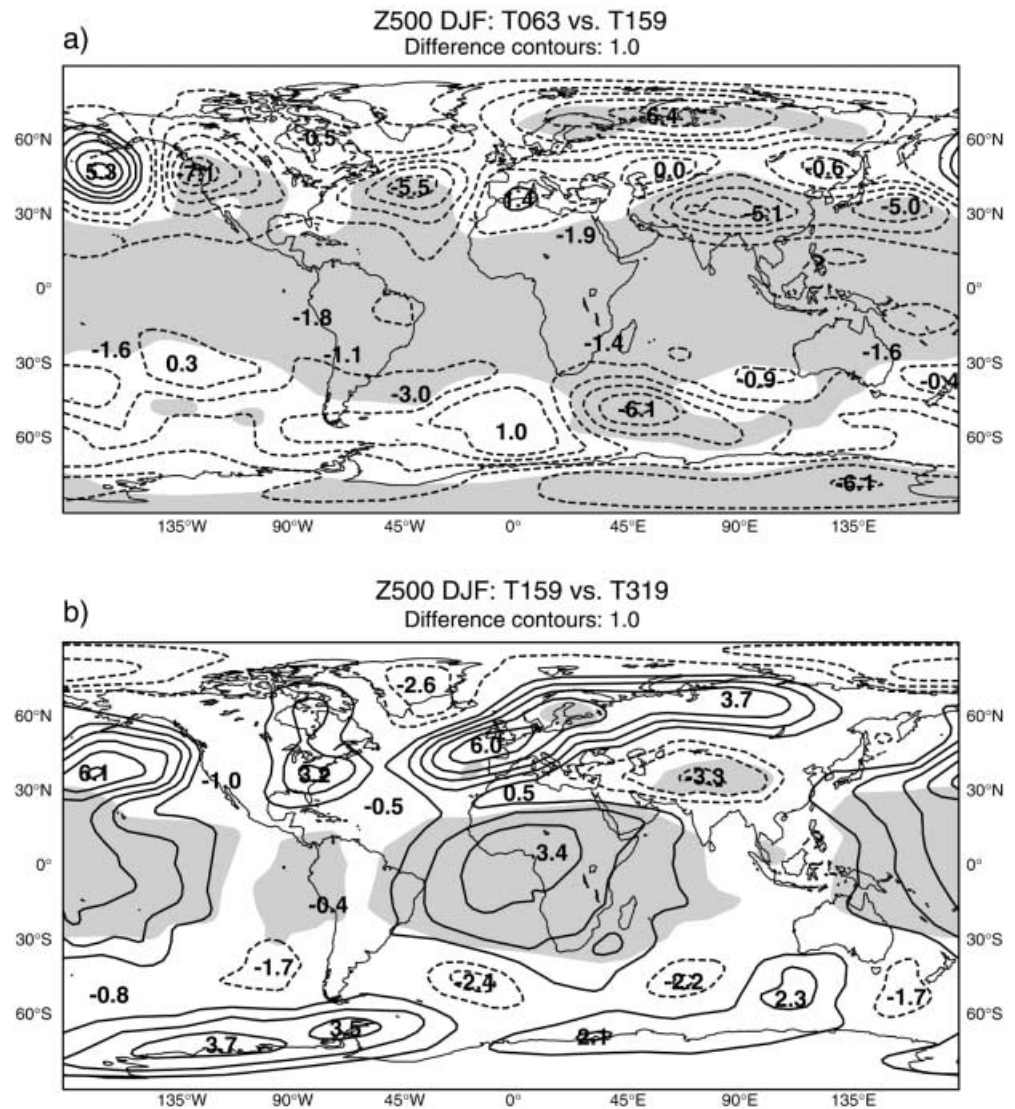
4 Statistical significance of differences between resolutions

A *t*-test was performed to establish how different the ensemble mean was at one resolution when compared with the ensemble mean at the other resolutions. Figure 8 shows the DJF 500 mb geopotential height difference field together with the spatial distribution of

t-values at the 95% confidence level when T63 and T_L159 are compared (Fig. 8a) and when T_L159 and T_L319 are compared (Fig. 8b). The difference fields in Fig. 8 and in subsequent figures with *t*-statistics are always computed in the sense of ‘lower resolution minus higher resolution’. Although the differences between T63 and T_L159 in the tropical regions (between 30°N and 30°S, Fig. 9a) are relatively small when compared to the extratropics (mainly less than 2 dam), the shading indicates that in a statistical sense they are highly significant. Outside the tropics there are many regions with significant differences: i.e. northern Europe and northern Asia, southern Asia, subtropical Atlantic, northwestern North America and the southern Indian Ocean. Most differences are of the negative sign indicating a warming of much of the extratropical troposphere at T_L159 relative to T63; relatively large positive differences over the north Pacific are not significant.

The difference between the two higher resolutions (Fig. 8b) is somewhat less statistically significant than that between T63 and T_L159. It is confined mainly to the tropics, the 95% confidence level being broken into several regions indicating a less coherent difference between the two high resolutions than that between T63 and T_L159. The relatively large differences over northern Europe seem to be just statistically significant. It is interesting to note that in both panels of Fig. 8 the differences over the Tibetan Plateau are highly significant, indicating an important impact of changing orography with resolution on the 500 mb height field over that region. However, the differences are not significant over

Fig. 8a, b Differences and *t*-statistic of the DJF 1987/88 500 mb geopotential height for the comparison of **a** T63 minus T_L159, and **b** T_L159 minus T_L319. Difference contours 1 dam; negative differences dashed. Shading is for the 95% confidence level



some other areas with high orography (such as the Rockies), indicating that the T_L159 model may be adequate there.

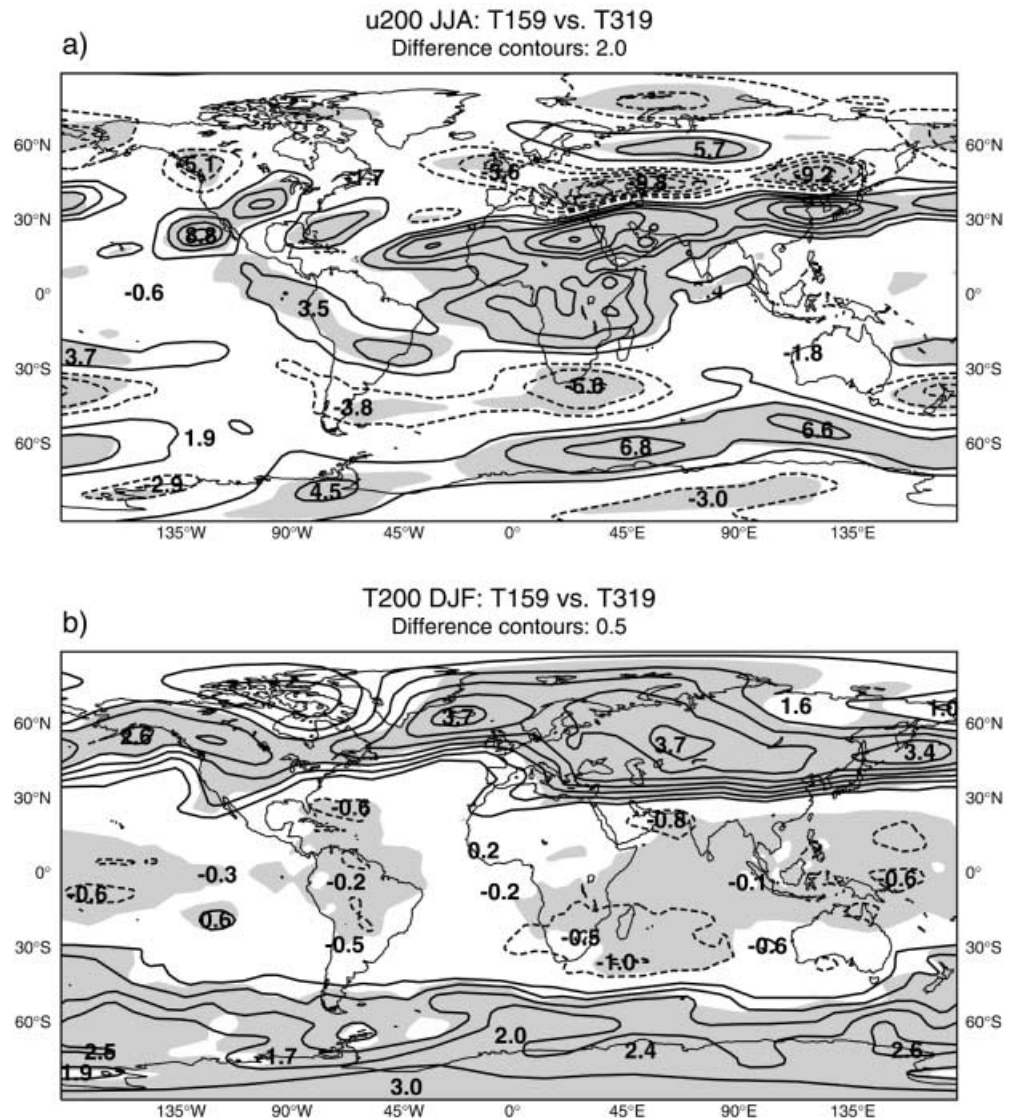
For JJA, similar results to those seen for DJF are evident, in particular for the T63 versus T_L159 comparison (not shown), but some variations exist. For the T_L159 versus T_L319 comparison the 95% significance level is found over much of southern Asia, with differences of nearly 8 dam in the region of the Persian Gulf. However, for the T63 versus T_L159 comparison the 95% threshold does not cover the Arabian Sea and Middle East (it is even below 80%), i.e. these two resolutions do not differ significantly over that region. This indicates relatively large differences in the representation of the Indian summer monsoon with higher resolutions. Indeed, the low level flow at 850 mb over the Arabian Sea is very similar at T63 and T_L159 (and relatively close to ERA-15), but is strengthened at T_L319 (not shown; see also the discussion on monsoon precipitation in Sect. 6.1). These results suggest that the resolution increase might affect different flows in different ways, but

may also indicate a possible sensitivity of parametrization to changes in resolution.

For *u*-wind at 200 mb, the largest differences were found between T_L159 and T_L319 in JJA over the African-Indian region (Fig. 9a). This is the consequence of an overestimation of easterlies at T_L319; the maximum error over the eastern Africa reaches 12 ms⁻¹ at T_L319 compared to a half of that amplitude at T_L159 (see also Fig. 3 right panels). This is in agreement with more intense precipitation during the Indian summer monsoon seen in the T_L319 model. The negative and partly statistically significant differences over the north Atlantic and across central and eastern Europe in Fig. 9a indicate a somewhat stronger and broader subtropical jet over these regions in T_L319 relative to T_L159. This has an implication on the European summer precipitation rates in the high-resolution model (see Sect. 6.1).

In Sect. 3.3, large Northern Hemisphere differences in temperature at 200 mb between T_L319 and other model resolutions were discussed (Fig. 7). This is also seen in Fig. 9b where these large differences between

Fig. 9a, b As Fig. 8 but for the comparison of T_{L159} minus T_{L319} for **a** JJA 1987 200 mb u -wind, and for **b** DJF 1987/88 200 mb temperature. Difference contours 2 ms^{-1} in **a**, and 0.5 K in **b**; negative differences dashed. Shading for the 95% confidence level



T_{L159} and T_{L319} (of nearly 4 K) are marked by the 95% significance level. Statistically significant differences are also found over much of the tropics and in the Southern Hemisphere.

5 Tropical circulation

In this section we focus on the dynamics of the large-scale tropical circulation. Because of its intrinsic links with other spatial scales, some large-scale circulation effects on smaller scales will be discussed here. However, a more detailed discussion on precipitation rates and other surface parameters is given in Sect. 6.

5.1 Vertical motion

Considering the zonal mean meridional circulation in the tropics (not shown), all the resolutions overestimate

the Hadley cell relative to ERA-15. The error is largest at T63, gradually decreasing with resolution. Irrespective of season, the largest contribution to this error comes primarily from model's overestimation of the large-scale tropical ascent. However, it has to be noted that this type of error may depend to a great extent on the formulation of model physics (see, e.g., Branković and Molteni 1997). The physical parametrization in the ECMWF model has undergone a series of changes between cycle 13R4 (introduced in operations in April 1995 and used for ERA-15) and cycle 18R6 used for these experiments. Therefore, a cautious approach has to be exercised when verifying forecast data that are primarily driven by model physics.

Some details of the 500 mb spatial distribution of the tropical vertical velocity are shown in Fig. 10. In DJF (left panels), the largest area of a relatively strong ascent over the Pacific warm pool region is found at T_{L319} . Since the SSTs were identical in all the resolutions considered, this implies that the highest resolution is

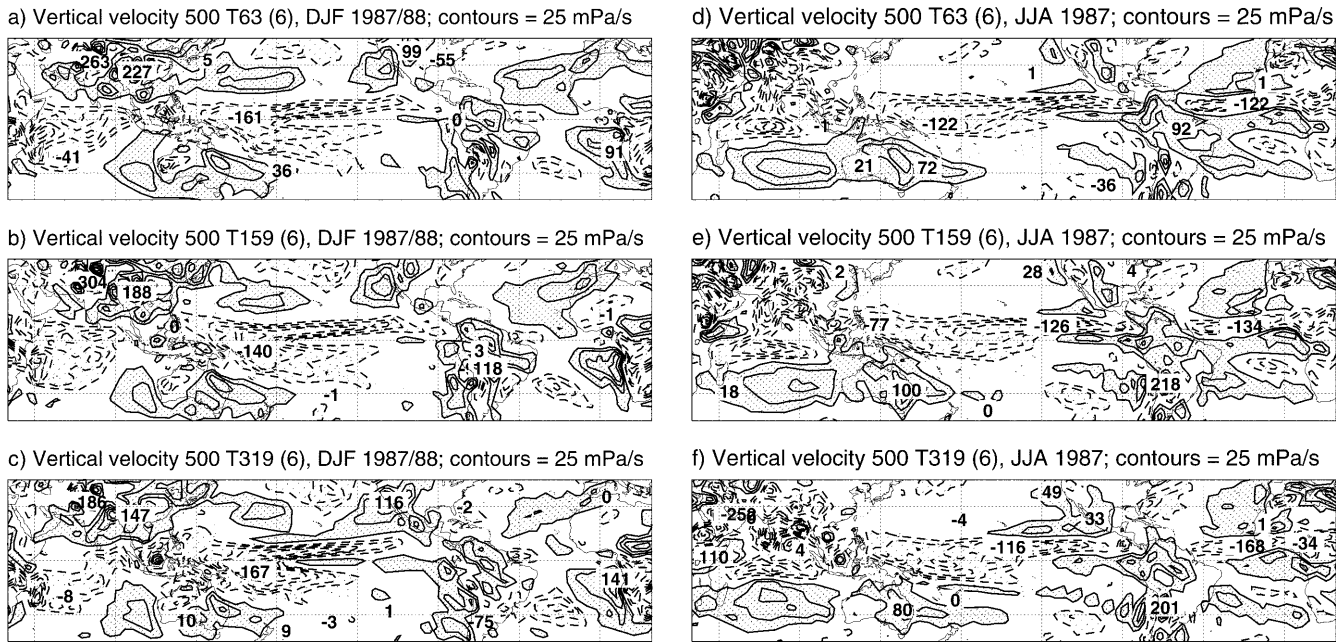


Fig. 10a–f Tropical 500 mb vertical velocity in DJF 1987/88 (left) and JJA 1987 (right) for T63 (top), T_{L159} (middle) and T_{L319} (bottom). Contours: 25 mPa⁻¹. Rising motion coarse stipple (dashed), sinking motion dense stipple (solid)

reacting more strongly to the forcing from the boundary imposed by prescribed SST. In all resolutions, a narrow area of descent is seen in the central equatorial Pacific situated in between the two branches of rising motion of the inter-tropical convergence zone (ITCZ) and the south Pacific convergence zone (SPCZ) respectively, this feature being the most prominent in the T_{L319} model. In contrast, a relative strong ascent over the western Indian Ocean decreases with increased resolution.

As the DJF rising motion in the SPCZ becomes stronger with resolution, it also increases in the region between northern Australia and Papua/New Guinea. Although this brings some increase in total cloudiness at T_{L319} over northern Australia, only a slight increase in monsoon precipitation occurs (not shown).

The largest discrepancy between the model simulations (regardless of the resolution) and ERA-15 in terms of the 500 mb vertical motion is found over the northern part of South America in DJF. Whereas in ERA-15 a rising motion is dominant over this region (not shown), in the model a relatively strong descent is seen (Fig. 10 left). Though this descent is manifested in a somewhat reduced cloud cover, the model precipitation rate over this region as verified against the Xie-Arkin data (Xie and Arkin 1997) is reasonable, thus indicating that ERA-15 may not be reliable in this case.

In JJA (Fig. 10, right panels), the T_{L319} displays the most structured and detailed ascent over the Indian monsoon region, including the Bay of Bengal. However, this is not necessarily the most accurate model simulation. As discussed later, at T_{L319} the Indian monsoon precipitation rates exceed substantially observed values. On the other hand, over the western equatorial Pacific, the rising motion is somewhat weakened at T_{L319} when

compared with both T63 and T_{L159} . The impact on precipitation is seen in Fig. 14; at T_{L319} , reduced amounts of precipitation over the South China Sea are seen relative to the other resolutions.

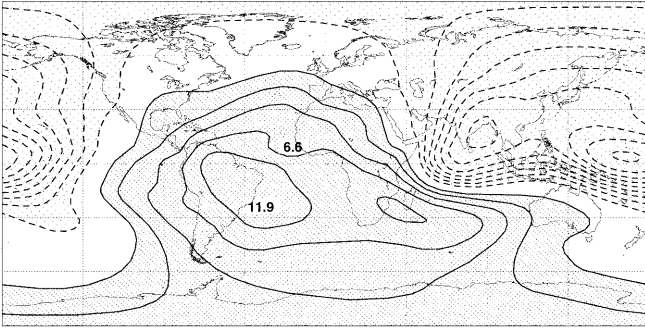
The Atlantic ITCZ is strongest with the T_{L319} resolution, as is the area of rising motion off the eastern coast of the United States, over the Gulf Stream. The latter may have important consequence on local atmospheric thermal stability that in turn may influence the maintenance and landfall of tropical cyclones in late summer.

5.2 Velocity potential and tropical variability

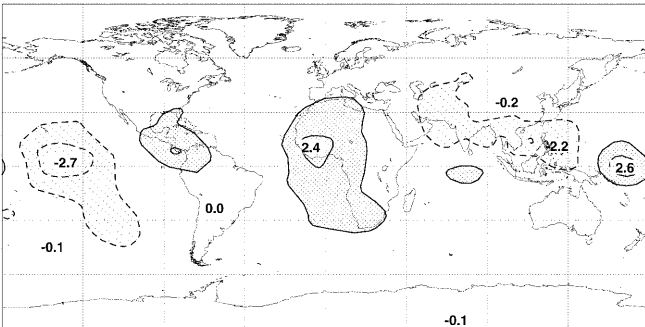
The large-scale tropical circulation is also shown in terms of velocity potential at 200 mb. Figure 11a shows the T63 full field, and Fig. 11b and c shows the difference between the higher resolutions and T63 respectively. (Note that differences in Fig. 11b and c are in the opposite sense to those in Fig. 8.) As for the 500 mb vertical velocity above, the results in Fig. 11 do not refer to ERA-15. Tropical precipitation appears to be sensitive to horizontal resolution (see Sect. 6.1) and the ECMWF convection scheme has undergone a major change from the time when ERA-15 data were made (see, e.g., Gregory et al. 2000). Therefore, velocity potential from ERA-15 may not be reliable for the verification when horizontal resolution is changed in the model.

We focus on the northern summer season, because the Walker circulation is, to a certain extent, related to the strength of the Indian monsoon. A negative difference over the South Asia indicates an increase in the maximum of upper air divergence at T_{L159} and T_{L319}

a) Velocity potential 200 T63 (6), JJA 1987; cont = 2



b) Velocity potential 200 T159-T63 (6), JJA 1987; cont = 1



c) Velocity potential 200 T319-T63 (6), JJA 1987; cont = 1

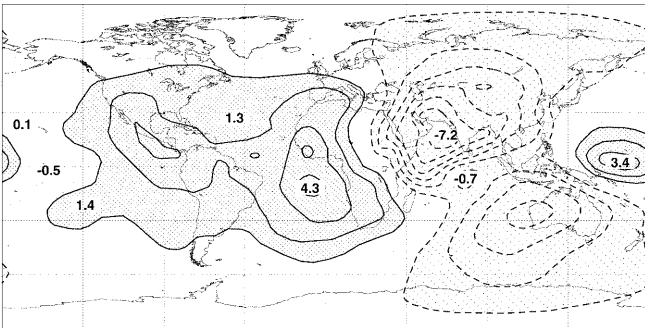


Fig. 11a–c JJA 1987 ensemble mean velocity potential at 200 mb. **a** T63 full field, **b** the difference between T_{L159} and T63, and **c** the difference between T_{L319} and T63. Contours: $2 \times 10^6 \text{ m}^2 \text{ s}^{-1}$ in **a**, and $1 \times 10^6 \text{ m}^2 \text{ s}^{-1}$ in **b** and **c**

relative to T63 with the outflow being much stronger at T_{L319} than at T_{L159} . This may be symptomatic of the model being over-responsive to SST anomalies of JJA 1987, in particular at higher resolutions (see similar result for an earlier version of ECMWF model in Palmer et al. 1992). The centre of the upper-air convergence has been strengthened and expanded from South America towards the African continent, again being much more intense at the highest resolution. Overall, although the pattern of the modelled large-scale tropical circulation is consistent among the resolutions considered, its intensity becomes larger as resolution increases.

The tropical (total) variability is also affected by the change in horizontal resolution. Figure 12 shows standard deviation of the 850 mb relative vorticity for JJA for the three resolutions and ERA-15. While Gregory

et al. (2000) indicate uncertainty in the use of this quantity diagnosed from ERA-15, in that it may underestimate tropical variability, the T63 model, and to a lesser extent T_{L159} , clearly underestimate variability in the low-level vorticity field in terms of spatial coverage and intensity. Although at T_{L319} there are some disagreements in details with ERA-15, the overall representation of variability over much of the tropics is improved over the lower resolutions. For DJF, similar results are found (not shown).

Previous studies have found that tropical variability is sensitive to the nature of the convection scheme (see, e.g., Slingo et al. 1994; Gregory et al. 2000). These studies suggested that the comparison between simulated and analyzed measures of variability is a useful indication whether the performance of the convection scheme is reasonable. However, they used resolution of T63 or lower. The great sensitivity of simulated tropical variability to increasing resolution, as demonstrated in Fig. 12, suggests that care must be exercised when interpreting the nature of such studies.

The day-to-day variability of the 200 mb velocity potential during the DJF 1987/88 season was also analyzed by using Hovmöller diagrams. This diagnostic is representative of the Madden-Julian oscillation (MJO; Madden and Julian 1971). In the verifying analysis, the two bursts of the upper-air divergent outflow can be identified moving eastward between 45°E and 150°E over the period of approximately 40 days (not shown). Neither resolution was able to reproduce this type of variability in the large-scale tropical flow. This result suggests a requirement, irrespective of horizontal resolution, for further reduction of model tropical errors before reliable tropical intraseasonal variability can be attained.

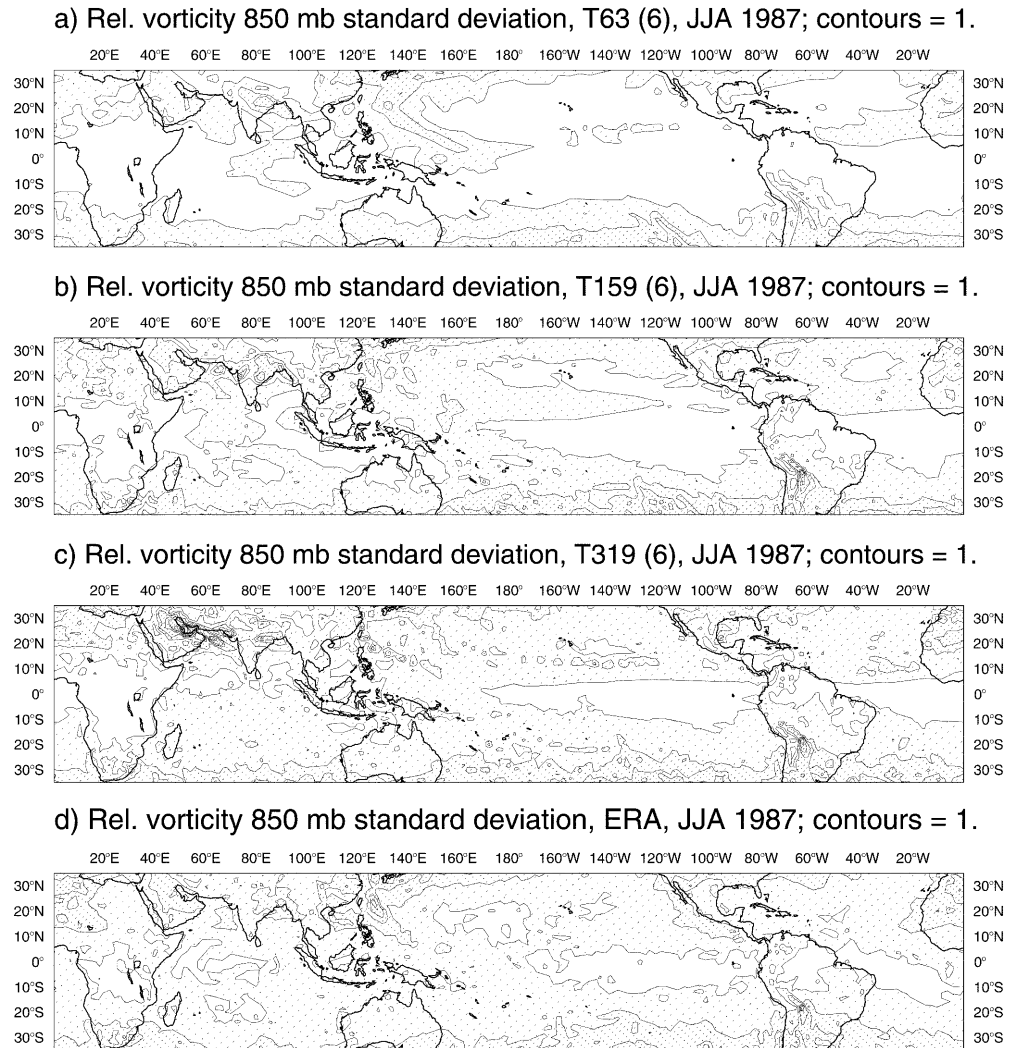
6 Surface fields

6.1 Precipitation

Figure 13 shows seasonal mean precipitation in mm day^{-1} for DJF (left) and JJA (right) over the European region. For both seasons, a gradual increase in precipitation amounts is seen as the resolution increases. This is evident almost all over the continent and parts of eastern Atlantic. Such an increase in precipitation can be in many places related to a better resolved orographic features (e.g. the Alps, the Caucasus, the Norwegian, Scottish and Albanian mountains). However, it is also seen in some areas where the orography is either featureless or nonexistent (e.g. eastern Europe, Finland, Russia, the North Sea).

In both seasons, the large-scale precipitation is the main contributor to such an overall precipitation increase (not shown), convective precipitation contributes comparatively much less. In DJF, slightly more than 2 mm day^{-1} over the Atlantic and the Mediterranean is convective in nature, whilst in JJA, convective precipi-

Fig. 12a–d Standard deviation of the JJA 1987 850 mb relative vorticity for **a** T63, **b** T_L159, **c** T_L319 and **d** ERA-15. Contours: $1 \times 10^6 \text{ s}^{-1}$



tation is important over the continental region only and is more widespread at T63 than at T_L319 resolution. The latter indicates the refinements and inclusion of relatively small-scale features in the representation of orography at T_L319. An increase in the JJA total precipitation at T_L319 relative to T_L159 over some parts of Europe is consistent with a relative strengthening of the subtropical jet (and the Atlantic storm track) in the high resolution model (see Sect. 4 and Fig. 9a).

The increase in precipitation with resolution has been also noted in some previous studies, for example, Jones et al. (1995) and Stratton (1999). In the former, a regional climate model of similar resolution to T_L319 covering the eastern north Atlantic and Europe was compared to a low-resolution climate model. The increase in precipitation was attributed to a larger vertical velocity at higher resolution. This is consistent with increased low-level moisture convergence. The additional effect of such an intensified hydrological cycle was also seen in increased tropospheric temperatures (see our discussion in Sect. 3.3).

In our experiments, the southern branch of the DJF 850 mb moisture flux, which penetrates from the Atlantic

into Spain and further over southern Europe, the Mediterranean and into the Black Sea is strongest in the T_L319 ensemble (not shown). The northern branch, which forks before reaching the Alps from its southern counterpart into the central and northern Europe, is very similar in all resolutions. However, at T_L319 a somewhat stronger moisture flux *convergence* over eastern Europe may have contributed to a larger precipitation rates in that region when compared with the other two resolutions. In JJA, the 850 mb moisture flux over central and eastern Europe is again strongest at T_L319 and may be linked with increased precipitation there.

For the verification of precipitation the data of Xie and Arkin (1997) were used. Seasonal averages were derived from monthly means for appropriate years. Whereas in DJF the T63 and T_L159 resolutions are relatively close to the verification data, with a drier eastern Europe and a wetter western Europe, in JJA, the T_L319 seems to fit best these verification estimates (Fig. 13, bottom panels). Over the north Atlantic, the model consistently overestimates precipitation.

Considering the Asian subcontinent, the maximum in the monsoon precipitation over western India and the

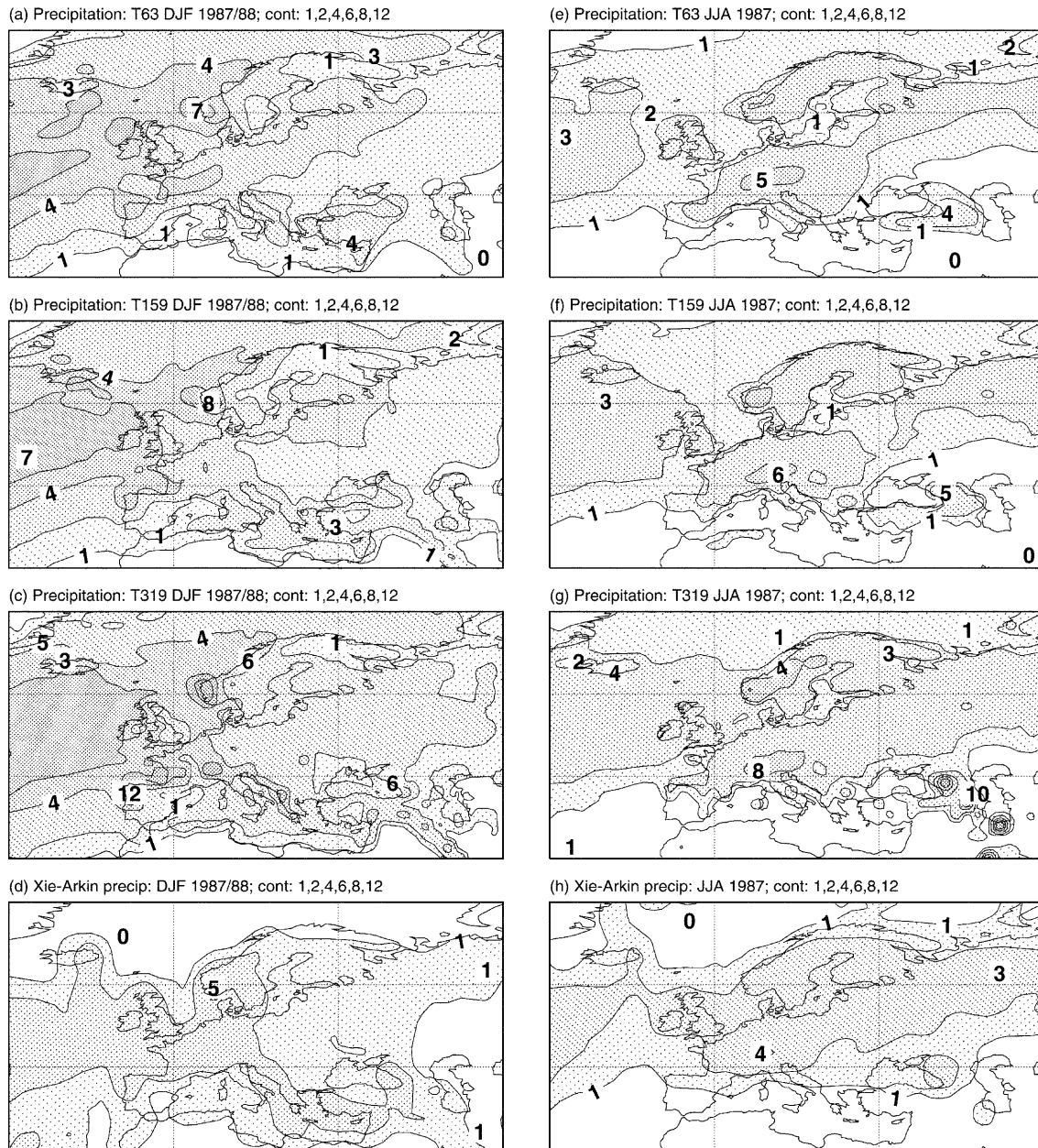


Fig. 13a-h European total precipitation in DJF 1987/88 (*left*) and JJA 1987 (*right*) from top to bottom: T63, T_L159, T_L319 and the Xie-Arkin data. Contours: 1, 2, 4, 6, 8, 12 mm day⁻¹

Bay of Bengal is doubled at T_L319 when compared with T63 (Fig. 14). Such a substantial increase may be ascribed to both better resolved orographic effects of the Western Ghats and an enhancement of the low level jet off the Somali coast in T_L319 (not shown; but see discussion in Sect. 4). When compared with the Xie-Arkin data (Fig. 14d), all resolutions overestimate Indian rainfall. On the other hand, in the Bay of Bengal, T63 underestimates, T_L319 overestimates, and T_L159 gives about right amount of precipitation.

The comparison of our results with earlier resolution studies (e.g. Tibaldi et al. 1990; Phillips et al. 1995; Sperber et al. 1994; Stephenson et al. 1998) is hampered

by the fact that, in most of these studies, the highest model resolution corresponds to our lowest resolution. Nevertheless, they do not report such a dramatic increase in the south Asian monsoon precipitation rates as the model resolution increases, and Phillips et al. (1995) even found monsoon precipitation somewhat reduced at higher resolutions. In most studies, the lowest resolution model (and usually this is T21) is most realistic in depicting the large-scale distribution and amounts of monsoon precipitation. The exception is the study by Lal et al. (1997), who found that the T106 model is superior to lower resolutions in realistically portraying spatial distribution of monsoon precipitation.

The zonally averaged precipitation in both seasons, for both model and Xie-Arkin precipitation data, is shown in Fig. 15. The T_L319 exhibits the largest zonally averaged precipitation rates of all resolutions. In midlatitudes, the difference between T_L319 and the other resolutions amounts to 1 mm day⁻¹. A relatively large difference in the belt between the equator and 10–15°S is mainly due to an increase in the SPCZ rainfall in the highest resolution model. A relatively good agreement among the models is found in high latitudes and during JJA in the region of ITCZ. The Xie-Arkin precipitation is consistently lower when compared with the model. The largest discrepancy between the model and verification can be seen in winter midlatitudes, up to 2 mm day⁻¹ for T_L319. All resolutions overestimate precipitation in the ITCZ, particularly in DJF. The consistency among resolutions and the agreement between the model and verification data is improved when only land points are considered (not shown). This may indicate that better representation of modelled precipitation is linked to orographic features.

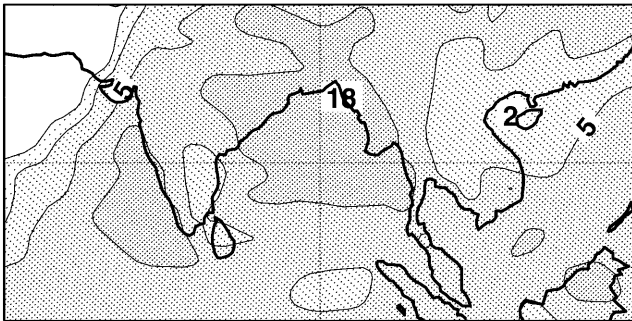
The *t*-statistic, discussed in Sect. 4 for upper-air fields, was also computed for precipitation. Irrespective of season, statistically significant differences between T63 and T_L159 resolutions are found mainly in the tropical and subtropical regions, in particular in the eastern Pacific off the coasts of Central and South America (not shown). The latter is associated with low stratiform cloud decks and very little or no precipita-

tion; small increases in cloud cover at T_L159 and negligible increases in precipitation contribute to high *t*-values over these regions. The significant differences between T_L159 and T_L319 are more widespread, and in addition to the tropics cover many parts of the extra-tropics, such as, the northern and southern storm track regions.

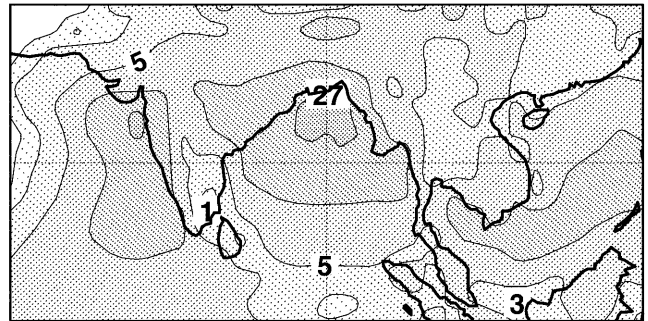
In Fig. 16 the *t*-statistic and precipitation differences are shown for the Indian summer monsoon (left) and for Europe in DJF (right). As before, the 95% confidence level is shown in both regions. Apart from the Himalayas and Tibetan Plateau, the largest and statistically significant precipitation differences in the Indian monsoon region, for both pairs of resolutions, are found over the Arabian Sea and the Bay of Bengal and adjacent coastal areas. The differences in inland India are not statistically significant, though they reach locally up to 5 mm day⁻¹. On the other hand, the higher rainfall amounts along the equator produced by the T63 resolution are significantly different from those found at T_L159.

Over Europe, the T63 versus T_L159 comparison yields in general relatively little statistical significance. For T_L159 versus T_L319 comparison, greater winter precipitation with the higher resolution is significant over much of the continent. However, this should not be considered to be only caused by a better representation of orography at T_L319, shaded areas being also found over the Atlantic and much of the eastern European flatlands (see also earlier discussion).

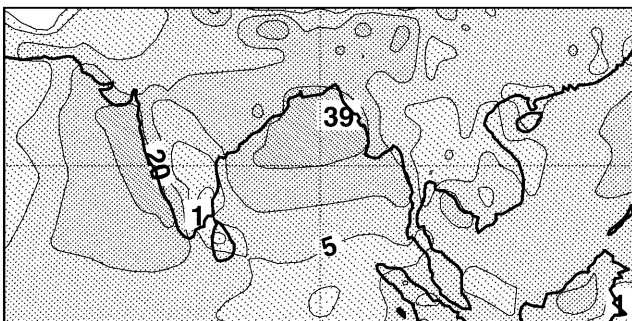
(a) Precipitation: T63 JJA 1987; cont: 1,2,5,10,20,50



(b) Precipitation: T159 JJA 1987; cont: 1,2,5,10,20,50



(c) Precipitation: T319 JJA 1987; cont: 1,2,5,10,20,50



(d) Xie-Arkin precip: JJA 1987; cont: 1,2,5,10,20,50

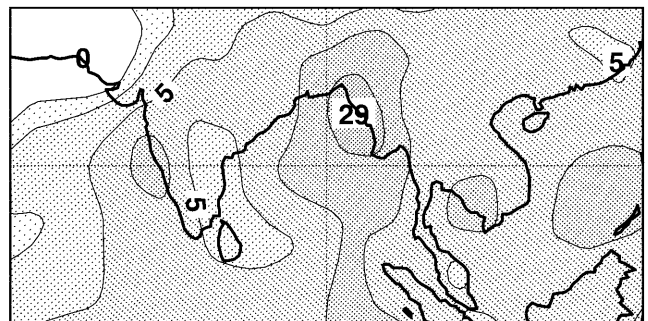


Fig. 14a–d South Asian total precipitation in JJA 1987 for **a** T63, **b** T_L159, **c** T_L319, and **d** Xie-Arkin data. Contours: 1, 2, 5, 10, 20, 50 mm day⁻¹

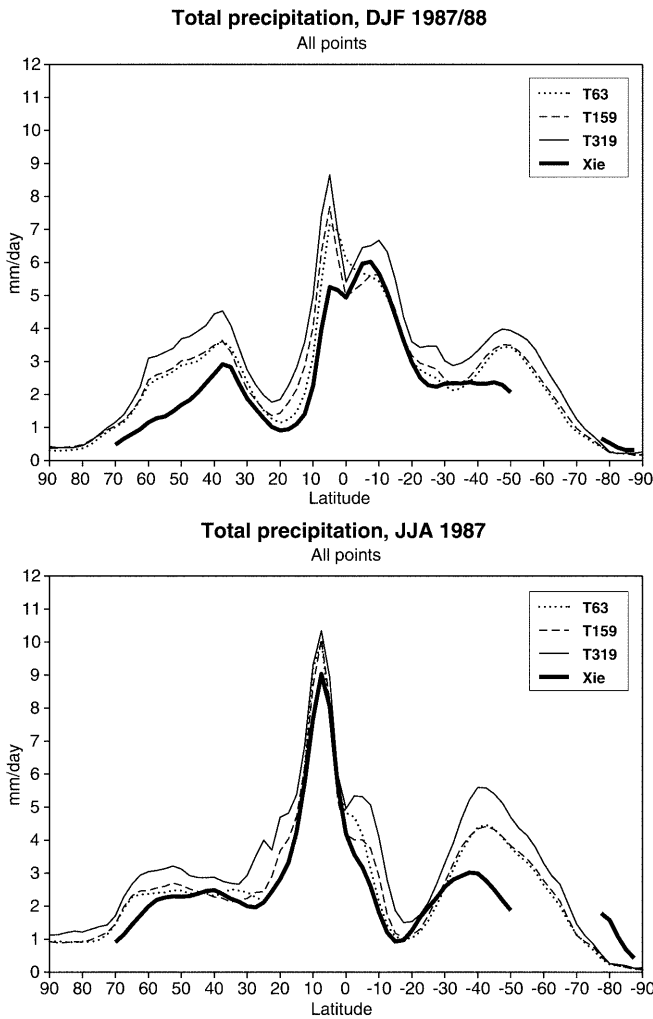


Fig. 15 Zonally averaged total precipitation in mm day^{-1} for DJF 1987/88 (top) and JJA 1987 (bottom). Xie and Arkin data heavy solid, T63 dotted, T_{L159} dashed and T_{L319} thin solid line

6.2 Surface fluxes and wind stress

The net surface thermal balance over sea points changes little as the resolution increases. In DJF, the heat deficit is 13, 10 and 12 W m^{-2} for T63, T_{L159} and T_{L319} respectively; in JJA, a heat surplus of 19, 21 and 24 W m^{-2} respectively is seen (see Table 2). This small variation across different resolutions is somewhat misleading, since for T_{L319} a strong compensating effect between different components takes place. At T_{L319} , both surface latent heat flux and thermal radiation (both negative) and surface solar radiation (positive) exhibit an increase in amplitude relative to the lower resolutions. The only component of the thermal balance that remains essentially unchanged at T_{L319} when compared with the other resolutions is surface sensible heat flux. Therefore, the overall effect of these (opposite) flux increases at T_{L319} is that the net surface flux at the highest resolution is rather similar to that at T63 and T_{L159} .

The DJF surface wind stress in the north Pacific winter storm track is monotonically enhanced from T63

to T_{L319} (Fig. 17). In the region of the northern trade winds, there is very little change in stress with resolution. In the southern (less important) trades, wind stress is reduced at T_{L159} relative to T63, and at T_{L319} , is increased again. Similar behaviour is also found in the Indian Ocean in both seasons. This increase in surface wind stress at T_{L319} is associated with an increase in (oceanic) surface evaporation rates relative to the other resolutions (not shown).

7 Conclusions

The impact of horizontal resolution on seasonal time scales has been studied from ensembles of integrations made with a relatively recent version of the ECMWF model. The model was integrated at T63, T_{L159} and T_{L319} spectral resolution; the latter effectively corresponds to 0.56° latitude/longitude grid. Thus, the study considerably extends the range of resolutions for which comparable experimentation has been carried out by other authors. The six-member ensembles were run for one winter and one summer season. Whereas one winter and one summer are by no means sufficient to evaluate model biases fully, they nevertheless give a valuable insight on the influence of horizontal resolution on seasonal time-scales.

The general impression is that there are no dramatic differences in simulated ensemble averages among the three resolutions considered, i.e. for most parameters, circulation and error patterns are similar. Also, no clear pattern of either improvement or deterioration emerged as the horizontal resolution changes. However, differences among the resolutions exist and are mostly in the detail rather than characterizing the large-scale flow. In some cases a direct relationship between improved representation of orography, as the horizontal resolution increases, and changed circulation feature can be concluded (like increased winter precipitation rates over parts of Europe). However, some differences cannot be always attributed to local differences in the representation of orography. Overall, the upper-air fields seem to benefit most from increased horizontal resolution. However, it is not clear if this is the case for surface fields.

When compared with some earlier resolution studies (e.g. Stratton 1999; Williamson et al. 1995), the following similarities as resolution increased were found: increase in tropical vertical motion, increase in eddy kinetic energy and warming of tropospheric mid-latitudes. In contrast, relatively small differences among the resolutions considered were found in eddy momentum and heat fluxes. The precipitation changes behaved differently over different parts of the globe, though, in general, increased precipitation in both DJF and JJA was found at higher resolutions.

Whereas some changes in the model response are not monotonic with the resolution increase from T63 to T_{L159} and to T_{L319} , there are some systematic changes

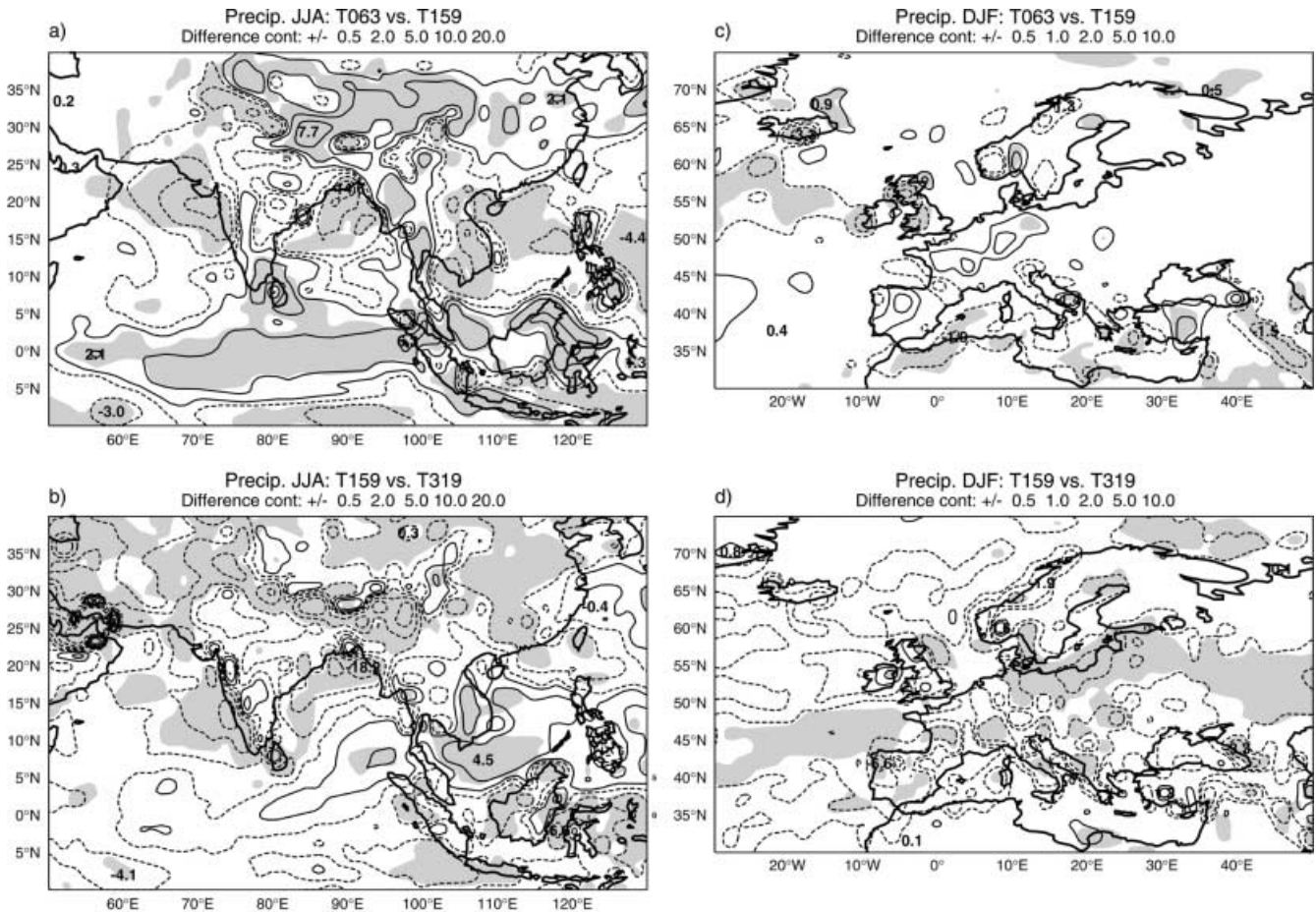


Fig. 16a–d As Fig. 8 but for JJA 1987 south Asian precipitation for the comparison **a** T63 minus T_{L159}, and **b** T_{L159} minus T_{L319}; for DJF 1987/88 European precipitation for the comparison **c** T63 minus

T_{L159}, and **d** T_{L159} minus T_{L319}. Difference contours $\pm 0.5, 2, 5, 10$ and 20 mm day^{-1} in **a** and **b**, and $\pm 0.5, 1, 2, 5$ and 10 mm day^{-1} in **c** and **d**; negative differences *dashed*. Shading for the 95% confidence level

Table 2 Surface energy components (in Wm^{-2})

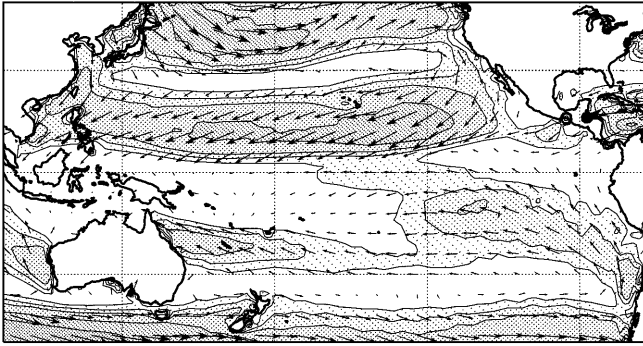
| Season | DJF | | | JJA | | |
|--------------------|------|-------------------|-------------------|------|-------------------|-------------------|
| | T63 | T _{L159} | T _{L319} | T63 | T _{L159} | T _{L319} |
| Sensible heat flux | -12 | -12 | -11 | -10 | -9 | -9 |
| Latent heat flux | -107 | -111 | -131 | -105 | -108 | -129 |
| Solar radiation | 186 | 187 | 216 | 148 | 147 | 174 |
| Thermal radiation | -54 | -54 | -62 | -52 | -52 | -59 |
| Net surface flux | 13 | 10 | 12 | -19 | -21 | -24 |

with resolution, especially in the tropics. These systematic differences between various resolutions question whether it is sufficient to rely solely on low-resolution simulations for model development and testing (a common practice adopted by many modelling centres), if one of the primary uses of a model is at higher resolution, such as deterministic forecasting in the medium-range. Differences in systematic errors with changing resolution imply that the use of low-resolution configurations in the process may not be optimal. Further reductions in errors at higher resolution may be possible by some adjustment of physical parametrizations. A long-term goal,

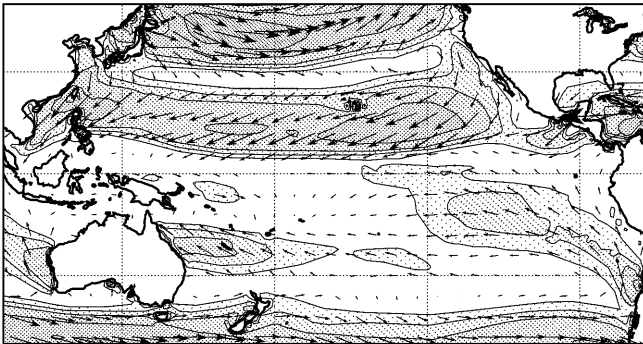
therefore, would be the development of parametrizations that are not sensitive to resolution (although this may be difficult to attain, as the performance of the model dynamics also changes with resolution). It should be noted that in the ECMWF model used here some parametrizations are adjusted to account for different behaviour of the dynamics as resolution changes. For example, the time scale over which the convection scheme adjusts thermodynamic profiles back to neutral is decreased as resolution increases, from 2 h at T63 to 25 min at T_{L319}, in response to increasing vertical velocity (Gregory et al. 2000).

As already noted by Williamson et al. (1995), increased resolution does not always lead to improved results. The prime example in this study is Indian summer monsoon precipitation, at T_{L319} being substantially overestimated when compared with observational data. On the other hand, whereas reanalysis data (either from ERA or other reanalyses) are invaluable for assessment of various aspects of model climatology, not all parameters from reanalyses are reliable for verification purposes. For example, vertical velocity depends strongly on model physical formulation, and so verifi-

Wind stress: T63 DJF 1987/88; Arrow unit 200 mPa; cont: 50,75,100,150,200,400



Wind stress: T159 DJF 1987/88; Arrow unit 200 mPa; cont: 50,75,100,150,200,400



Wind stress: T319 DJF 1987/88; Arrow unit 200 mPa; cont: 50,75,100,150,200,400

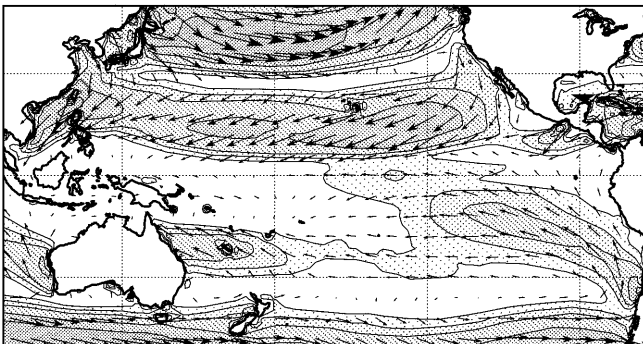


Fig. 17 DJF 1987/88 Pacific surface wind stress in mPas for T63 (*top*), T_L159 (*middle*) and T_L319 (*bottom*) resolutions. Contours: 50, 75, 100, 150, 200, 400 mPas

cation of a different version of the same model with reanalysis data may lead to erroneous conclusion about model systematic error.

Acknowledgements We thank Nils Wedi for his help in setting up the T_L319 resolution experiments and Laura Ferranti for producing the MJO diagnostics. Comments and suggestions by Martin Müller and Tim Palmer are highly appreciated. We also thank two anonymous referees whose comments and suggestions improved the original version of the paper.

References

Boer GJ, Lazare M (1988) Some results concerning the effect of horizontal resolution and gravity-wave drag on simulated climate. *J Clim* 1: 789–806

- Boer GJ, Arpe K, Blackburn M, Déqué M, Gates WL, Hart TL, Le Treut H, Rockner E, Sheinin DA, Simmonds I, Smith RNB, Tokioka T, Wetherald RT, Williamson D (1991) An inter-comparison of the climates simulated by 14 atmospheric general circulation models. CAS/JSC Working Group on Numerical Experimentation, Rep 15, WMO/TD-425
- Boyle JS (1993) Sensitivity of dynamical quantities to horizontal resolution for a climate simulation using the ECMWF (cycle 33) model. *J Clim* 6: 796–815
- Branković Č, Molteni F (1997) Sensitivity of the ECMWF model northern winter climate to model formulation. *Clim Dyn* 13: 75–101
- Branković Č, Palmer TN (1997) Atmospheric seasonal predictability and estimates of ensemble size. *Mon Weather Rev* 125: 859–874
- Branković Č, Palmer TN (2000) Seasonal skill and predictability of ECMWF PROVOST ensembles. *Q J R Meteorol Soc* 126: 2035–2067
- Déqué M, Piedelievre JPh (1995) High resolution climate simulation over Europe. *Clim Dyn* 11: 321–339
- Gibson JK, Kållberg P, Uppala S, Nomura S, Hernandez A, Serrano E (1997) ERA description. ECMWF Re-Analysis project Report Series 1
- Gregory D, Morcrette J-J, Jakob C, Beljaars A, Stockdale T (2000) Revision of convection, radiation and cloud schemes in the ECMWF Integrated Forecasting System. *Q J R Meteorol Soc* 126: 1685–1710
- Hortal M (1999) The development and testing of a new two-time-level semi-Lagrangian scheme (SETTLS) in the ECMWF forecast model. ECMWF Tech Memo 292
- Hortal M, Simmons AJ (1991) Use of reduced Gaussian grids in spectral models. *Mon Weather Rev* 119: 1057–1074
- Janssen PAEM, Viterbo P (1996) Ocean waves and the atmospheric climate. *J Clim* 9: 1269–1287
- Johnson DR (1997) “General coldness of climate models” and the second law: implications for modeling the Earth system. *J Clim* 10: 2826–2846
- Jones RG, Murphy JM, Noguer M (1995) Simulation of climate change over Europe using a nested regional-climate model. I: assessment of control climate, including sensitivity to location of lateral boundaries. *Q J R Meteorol Soc* 121: 1413–1449
- Lal M, Cubasch U, Perlwitz J, Waszkewitz J (1997) Simulation of the Indian monsoon climatology in ECHAM3 climate model: sensitivity to horizontal resolution. *Int J Climatol* 17: 847–858
- Lorenz EN (1967) The nature and theory of the general circulation of the atmosphere. WMO, Geneva, p 161
- Madden RA, Julian PR (1971) Detection of a 40–50 day oscillation in the zonal wind in the tropical Pacific. *J Atmos Sci* 28: 702–708
- Palmer TN, Branković Č, Viterbo P, Miller MJ (1992) Modelling interannual variations of summer monsoons. *J Clim* 5: 399–417
- Palmer TN, Shutts GJ, Swinbank R (1986) Alleviation of a systematic westerly bias in general circulation and numerical weather prediction models through an orographic gravity wave drag parameterisation. *Q J R Meteorol Soc* 112: 1001–1039
- Phillips TJ, Corsetti LC, Grotch SL (1995) The impact of horizontal resolution on moist processes in the ECMWF model. *Clim Dyn* 11: 85–102
- Slingo JM, Blackburn M, Betts A, Brugge R, Hodges K, Hoskins B, Miller M, Steenman-Clark L, Thurnburn J (1994) Mean climate and transience in the tropics of the UGAMP GCM: sensitivity to convective parametrization. *Q J R Meteorol Soc* 120: 881–922
- Sperber KR, Hameed S, Potter GL, Boyle JS (1994) Simulation of the northern summer monsoon in the ECMWF model: sensitivity to horizontal resolution. *Mon Weather Rev* 122: 2461–2481
- Stephenson DB, Chauvin F, Royer J-F (1998) Simulation of the Asian summer monsoon and its dependence on model horizontal resolution. *J Meteorol Soc Japan* 76: 237–265
- Stratton RA (1999) A high resolution AMIP integration using the Hadley Centre model HadAM2b. *Clim Dyn* 15: 9–28

- Tibaldi S, Molteni F (1990) On the operational predictability of blocking. *Tellus* 42A: 343–365
- Tibaldi S, Palmer TN, Branković Č, Cubasch U (1990) Extended-range predictions with ECMWF models: influence of horizontal resolution on systematic error and forecast skill. *Q J R Meteorol Soc* 116: 835–866
- Williamson DL, Kiehl JT, Hack JJ (1995) Climate sensitivity of the NCAR Community Climate Model (CCM2) to horizontal resolution. *Clim Dyn* 11: 377–397
- Xie P, Arkin PA (1997) Global precipitation: a 17-year monthly analysis based on gauge observations, satellite estimates and numerical model outputs. *Bull Am Meteorol Soc* 78: 2539–2558